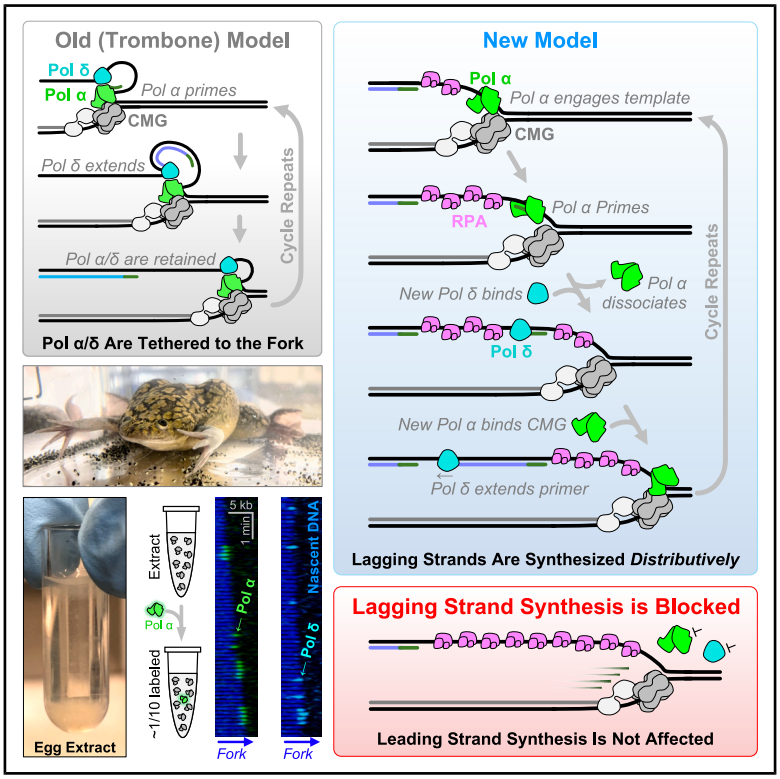
Cell

Short article

Metazoan lagging-strand DNA synthesis is distributive

Graphical abstract



Highlights

- Single-molecule imaging reveals dynamic lagging-strand replication
- Pol α and Pol δ are exchanged rather than recycled at replication forks
- New polymerases are recruited for each round of Okazaki fragment synthesis
- Leading- and lagging-strand synthesis are not intrinsically coupled

Authors

Luke D. Lynch, Jinho Park, Gheorghe Chistol

Correspondence

chistol@stanford.edu

In brief

Single-molecule imaging reveals that metazoan lagging-strand DNA synthesis is distributive, and it relies on the repeated recruitment of Pol α and Pol δ rather than their stable replisome association, thereby uncoupling leading- and lagging-strand synthesis.

Lynch et al., 2026, Cell *189*, 1–12
December 24, 2026 © 2026 The Author(s). Published by Elsevier Inc.
https://doi.org/10.1016/j.cell.2026.09.060

CellPress

Please cite this article in press as: Lynch et al., Metazoan lagging-strand DNA synthesis is distributive, Cell (2026), https://doi.org/10.1016/j.cell.2026.09.060

Cell

CellPress
OPEN ACCESS

Short article

Metazoan lagging-strand DNA synthesis is distributive

Luke D. Lynch,[1,5] Jinho Park,[2] and Gheorghe Chistol[2,3,4,6,*]
[1]Biochemistry Department, Stanford School of Medicine, Stanford, CA 94305, USA
[2]Chemical and Systems Biology Department, Stanford School of Medicine, Stanford, CA 94305, USA
[3]Stanford Cancer Institute, Stanford School of Medicine, Stanford, CA 94305, USA
[4]BioX Interdisciplinary Institute, Stanford University, Stanford, CA 94305, USA
[5]Present addresses: Department of Biological Chemistry and Molecular Pharmacology, Blavatnik Institute, Harvard Medical School, Boston, MA, USA; Howard Hughes Medical Institute, Boston, MA 02115, USA
[6]Lead contact
*Correspondence: chistol@stanford.edu
https://doi.org/10.1016/j.cell.2026.09.060

SUMMARY

DNA's anti-parallel structure presents a topological challenge to the replisome, as leading and lagging strands must be synthesized in opposite directions. How lagging-strand synthesis is coordinated with leading-strand synthesis remains unresolved in eukaryotes. To address this question, we directly visualized the dynamics of lagging-strand polymerases Pol α and Pol δ at active replication forks using single-molecule imaging in *Xenopus* nuclear extracts. Surprisingly, we find that neither Pol α nor Pol δ is stably tethered to the replisome. Instead, lagging-strand synthesis occurs distributively and entails the rapid recruitment of new molecules of Pol α and Pol δ for each Okazaki fragment. Consequently, leading- and lagging-strand synthesis are not intrinsically coupled. We propose that metazoans solve the problem of anti-parallel replication not by actively coordinating leading- and lagging-strand synthesis, but instead simply by recruiting new polymerases to synthesize each Okazaki fragment.

INTRODUCTION

In eukaryotes, Polymerase ε (Pol ε) synthesizes the leading strand continuously, while Polymerase α-Primase (Pol α) and Polymerase δ (Pol δ) synthesize lagging-strand fragments discontinuously.[1–4] For a typical vertebrate with a 6-billion nucleotide (nt) genome, lagging-strand synthesis poses a monumental task, as ∼40 million Okazaki fragments (∼150 nt each) must be synthesized before each cell division. First, Pol α is recruited to the replicative helicase CMG (CDC45·MCM2-7·GINS) and engages the lagging-strand template.[5] Second, Pol α synthesizes a 6–10 ribonucleotide (rNTP) primer,[6] extends it by 20–30 deoxyribonucleotides (dNTPs), then disengages from the template.[7,8] Third, the proliferating cell nuclear antigen (PCNA) is loaded onto the primer-template junction, promoting the recruitment of Pol δ,[9] which extends the primer[10] until colliding with a downstream Okazaki fragment.[11] Finally, the flap endonuclease 1 (FEN1) cleaves the RNA primer and neighboring Okazaki fragments are ligated.[10] Primer-template junctions that form transiently during lagging-strand synthesis (or persistently during replication stress) activate the kinase ATR (ataxia-telangiectasia and Rad3-related)—the master regulator of the S-phase checkpoint.[12,13] ATR phosphorylates the effector kinase CHK1 (checkpoint kinase 1), which launches numerous cellular responses to safeguard genome integrity.[14]

Early studies of bacteriophage replication revealed that both the DNA primase and the lagging-strand DNA polymerase are stably tethered to the replisome, thus enabling it to processively synthesize many consecutive Okazaki fragments.[15,16] To rationalize this, it was proposed that the lagging-strand DNA template forms a trombone-like loop to facilitate the coordinated synthesis of leading and lagging strands by a single stable enzyme complex.

Although prokaryotic and eukaryotic replication machineries evolved independently,[17] the trombone model originally proposed for prokaryotes was adopted for eukaryotes. Two recent studies support the trombone model in yeast[18,19] (Figure 1A): an *in vitro* reconstitution study reported that Pol α/δ travel with the replisome for tens of minutes—long enough to synthesize hundreds of Okazaki fragments,[18] while another study imaged polymerases in live yeast and concluded that Pol α/δ are recycled for multiple Okazaki fragments.[19]

To elucidate the mechanism of lagging-strand synthesis in higher eukaryotes, we directly visualized Pol α/δ at active forks in *Xenopus* nuclear egg extract, which contains all soluble nuclear proteins and faithfully recapitulates replication.[20,21] Surprisingly, we find that Pol α/δ reside at active forks for only

This is an open access article under the CC BY license (http://creativecommons.org/licenses/by/4.0/).

Please cite this article in press as: Lynch et al., Metazoan lagging-strand DNA synthesis is distributive, Cell (2026), https://doi.org/10.1016/j.cell.2026.09.060

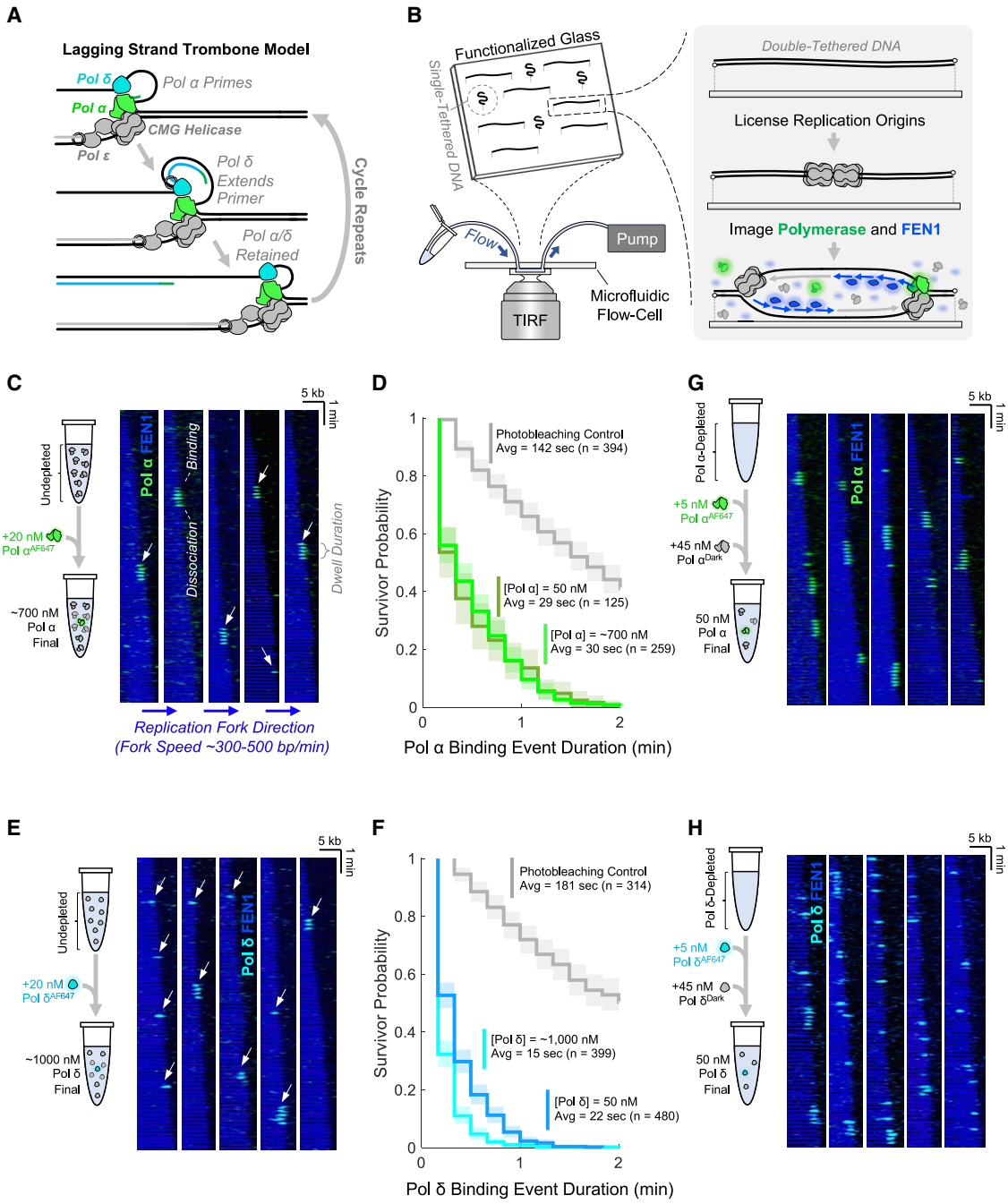


Figure 1. Pol α/δ are not stably tethered to the replisome

(A) Cartoon of the trombone model.

(B) Single-molecule experiment workflow.

(C) Kymograms of Pol α^{AF647} (green) and FEN1^{mKikGR} (blue) where 20 nM of Pol α^{AF647} was spiked into undepleted extract containing ~700 nM of endogenous Pol α.

(D) Survivor probability curves for Pol α^{AF647}-binding event duration. AF647 photobleaching times (gray) are much longer than Pol α^{AF647} residence time at forks (dark/light green).

(E) Kymograms of Pol δ^{AF647} (cyan) and FEN1^{mKikGR} (blue) where 20 nM of Pol δ^{AF647} was spiked in to undepleted extract containing ~1,000 nM of endogenous Pol δ.

(F) Survivor probability curves for Pol δ^{AF647}-binding event duration. Pol δ^{AF647} residence time at forks (dark/light blue) is much shorter than the photobleaching control (gray).

(legend continued on next page)

Please cite this article in press as: Lynch et al., Metazoan lagging-strand DNA synthesis is distributive, Cell (2026), https://doi.org/10.1016/j.cell.2026.09.060

15–30 s (whereas Pol α resides at stalled forks for several minutes). We find that the sudden removal of soluble Pol α and Pol δ from DNA replication reactions abruptly stops the synthesis of new Okazaki fragments. We show that blocking lagging-strand synthesis does not impair CMG progression, thus indicating that leading- and lagging-strand synthesis are not intrinsically coupled in metazoa. Our data support a "distributive" mechanism of lagging-strand replication, where new copies of Pol α/δ must be constantly recruited to the fork to sustain the synthesis of new Okazaki fragments.

RESULTS

Neither Pol α nor Pol δ are stably tethered to the replisome during unperturbed replication

The defining feature of the trombone model is that lagging-strand polymerases are stably tethered to the replisome and should travel with forks for several minutes (Figure 1A). To test this idea, we labeled recombinant Pol α/δ (Figures S1A and S1B) with Alexa-Fluor 647 and monitored the dynamics of Pol α^{AF647} and Pol δ^{AF647} at forks via single-molecule imaging in *Xenopus* egg extracts (Figure 1B).

We flow-stretched λ DNA and tethered it to a functionalized coverslip in a microfluidic flow-cell (Figure 1B). The flow-cell was incubated with *Xenopus* egg extracts that support efficient replication.[22] Extracts were supplemented with FEN1 fused to the fluorescent protein mKikGR (monomeric Kikume Green-Red) ($FEN1^{mKikGR}$), which serves as a marker of lagging-strand synthesis.[23]

First, we spiked 20 nM of Pol α^{AF647} into undepleted extract, which contains ~700 nM of endogenous Pol α. Pol α^{AF647} bound to elongating replisomes and resided at forks for ~30 s before dissociating (Figures 1C and 1D, light green). In egg extracts, forks travel at 300–500 nt/min and Okazaki fragments measure 100–500 nt,[24] therefore 30 s corresponds to 1–2 Okazaki fragments being synthesized. Although we did observe long-lived Pol α^{AF647} binding events, they were exclusively associated with stalled forks (Figures S1C and S1D).

Second, we spiked 20 nM of Pol δ^{AF647} into undepleted extract, which contains ~1,000 nM of endogenous Pol δ. We found that Pol δ^{AF647} transiently bound to elongating replisomes and resided at forks for only ~15 s (Figures 1E and 1F, light blue). Unlike Pol α, Pol δ was not retained at stalled forks (Figure S1E).

Short Pol α/δ residence times may reflect concentration-dependent exchange as reported for polymerases in yeast.[18] Endogenous Pol α (~700 nM) and Pol δ (~1,000 nM) concentrations in undepleted extract are comparable to Pol α (360–630 nM) and Pol δ (300–650 nM) concentrations reported in human cells.[25] To determine the lowest polymerase concentration that supports normal replication, we performed an ensemble replication assay and found that Pol α/δ concentrations above ~50 nM supported replication as well as undepleted extract (Figures S1F–S1I). Polymerase concentrations below 50 nM resulted in elevated pCHK1 levels relative to mock-depleted controls (Figures S1J and S1K).

To test whether polymerase exchange is concentration-dependent, we repeated the spike-in experiment using Pol α-depleted extract supplemented with 5 nM of Pol α^{AF647} and 45 nM of unlabeled Pol α (50 nM in total—the lowest concentration that supports normal replication). Lowering the Pol α concentration to 50 nM did not significantly change its residence time at the fork (Figures 1G and 1D, dark green).

We performed a similar experiment in Pol δ-depleted extract supplemented with 5 nM of Pol δ^{AF647} and 45 nM of unlabeled Pol δ and found that Pol δ^{AF647} bound to forks for only ~22 s (Figures 1H and 1F, dark blue). Pol δ's residence time is different from that of Pol α, which suggests that they do not form a stable complex as hypothesized previously.[26,27] Consistent with this, Pol α and Pol δ coimmunoprecipitated (coIP) only weakly (Figure S1L).

Stretching the DNA template in our experiments may disfavor the formation of trombone-like loops[15,16] and favor the separation of sister replisomes[28] (contrasting with reports that sister replisomes may remain physically coupled *in vivo*[29]). To address this, we measured the residence time of Pol α/δ on singly tethered DNA molecules that are not under tension. These DNAs are rapidly chromatinized and compacted into a diffraction-limited spot (Figure 1B, dotted circle). We found that Pol α/δ reside on replicating single-tethered DNA for ~43 s (Figures S1M–S1O) and 18 s (Figure S1P–S1R) respectively, consistent with the distributive mechanism. These data indicate that neither Pol α nor Pol δ reside at the fork long enough to synthesize several consecutive Okazaki fragments, regardless of their total concentrations.

Binding of a single copy of inactive Pol α/δ to the fork does not impair lagging-strand synthesis

The trombone model predicts that the incorporation of a single inactive Pol α/δ into the replisome should block lagging-strand synthesis for several minutes. To test this prediction, we generated catalytically dead Pol α (Pol α^{Dead}) by mutating its POLA1 subunit (D998S, D1000S) as described before[18] (Figure 2A). Notably, Pol α^{Dead} retains its RNA primase activity.[18] We verified that Pol α^{Dead} cannot rescue replication in a Pol α-depleted extract (Figures 2B and S2A). Spiking 20 nM of fluorescently labeled Pol α^{Dead} into undepleted extract revealed that it resides at forks as long as wild-type Pol α (Figures 2C and 2D). Importantly, the recruitment of Pol α^{Dead} to the replisome did not impair lagging-strand synthesis as monitored by growing $FEN1^{mKikGR}$ tracts (Figure 2C). We verified that the fluorescent tag does not affect Pol α's activity (Figures S2B and S2C).

Similarly, we generated catalytically dead Pol δ (Pol δ^{Dead}) by mutating POLD1 (D606A, D761A) as previously described[9] (Figure 2E). We confirmed that Pol δ^{Dead} cannot rescue replication in Pol δ-depleted extract (Figures 2F and S2D). Spiking

(G) Kymograms of Pol α^{AF647} (green) and $FEN1^{mKikGR}$ (blue) where 5 nM Pol α^{AF647} was spiked into Pol α-depleted extract supplemented with 45 nM unlabeled Pol α.

(H) Kymograms of Pol δ^{AF647} (green) and $FEN1^{mKikGR}$ (blue) where 5 nM Pol δ^{AF647} was spiked into Pol δ-depleted extract supplemented with 45 nM unlabeled Pol δ. In (D) and (F), boxes depict the 95% confidence interval (CI) estimated via bootstrapping; "*n*" denotes the number of events.

See also Figure S1.

Please cite this article in press as: Lynch et al., Metazoan lagging-strand DNA synthesis is distributive, Cell (2026), https://doi.org/10.1016/j.cell.2026.09.060

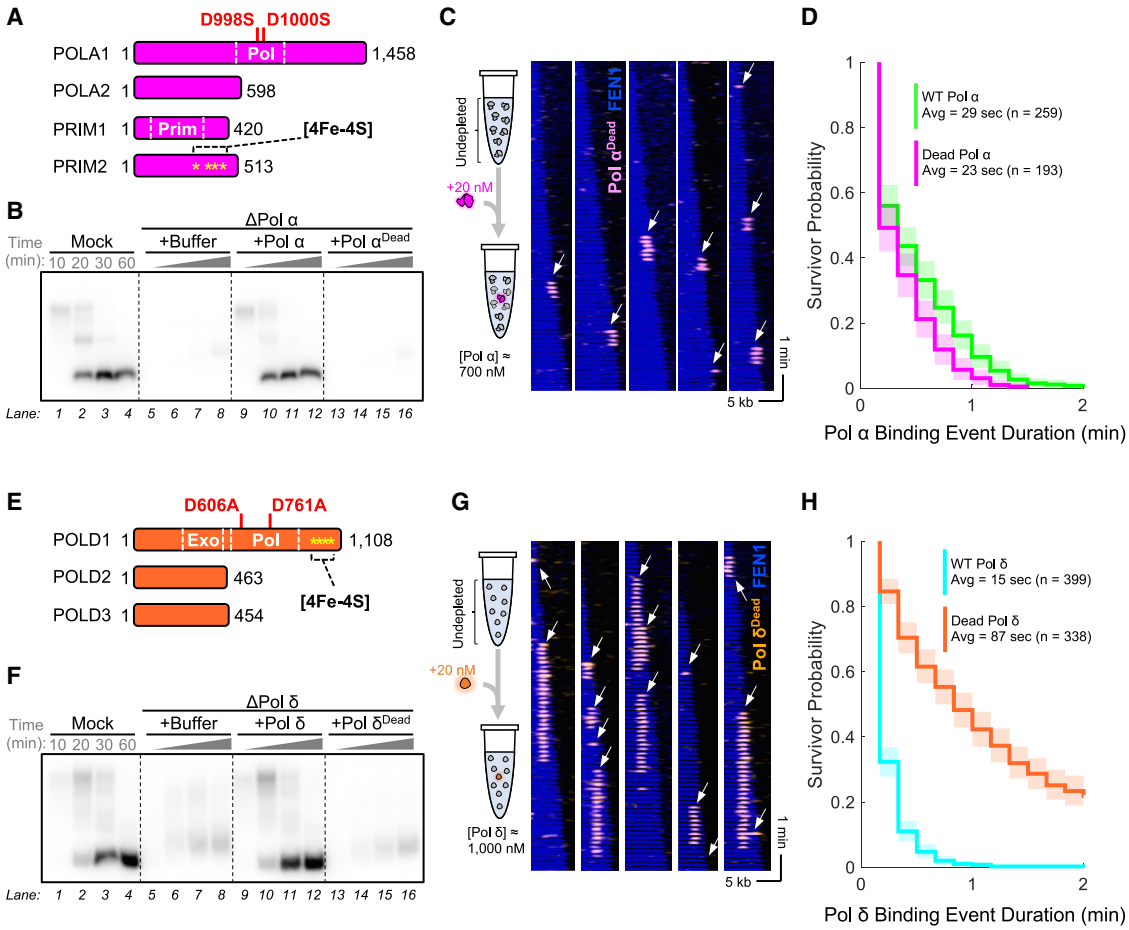


Figure 2. A single copy of catalytically dead Pol α/δ does not impair Okazaki fragment synthesis

(A) Diagram of catalytically dead *Xenopus* Pol α.

(B) Plasmid replication assay: Pol α-depleted extract was supplemented with 100 nM of recombinant Pol α^{WT} or Pol α^{Dead}.

(C) Kymograms where 20 nM of fluorescent Pol α^{Dead} (magenta) was spiked into undepleted extract containing ~700 nM of endogenous Pol α.

(D) Survivor probability curves of binding event duration for Pol α^{Dead} (magenta) versus Pol α^{WT} (green).

(E) Diagram of catalytically dead *Xenopus* Pol δ.

(F) Plasmid replication assay: Pol δ-depleted extract was supplemented with 100 nM of recombinant Pol δ^{WT} or Pol δ^{Dead}.

(G) Kymograms where 20 nM of fluorescent Pol δ^{Dead} (orange) was spiked into undepleted extract containing ~1,000 nM of endogenous Pol δ.

(H) Survivor probability curves for binding event duration: Pol δ^{Dead} (orange) versus Pol δ^{WT} (cyan). In (D) and (H), boxes depict the 95% CI; *n* denotes the number of events.

See also Figure S2.

20 nM of fluorescently labeled Pol δ^{Dead} into undepleted extract revealed that it binds to forks (Figure 2G) but resides on DNA much longer than wild-type Pol δ (Figure 2H). This is consistent with previous reports that human Pol δ^{Dead} dissociates from its template slowly.[9,30] We verified that the fluorescent tag does not affect Pol δ's activity (Figures S2E and S2F). Strikingly, although Pol δ^{Dead} initially bound to the edge of the FEN1^{mKikGR} bubble, Pol δ^{Dead} did not travel with the advancing fork (Figure 2G). This suggests that Pol δ is deposited behind the fork (Figure S2G) and corroborates the idea that Pol δ is not stably tethered to the replisome.

These findings indicate that the replisome can tolerate the recruitment of a single inactive Pol α/δ without impairing lagging-strand synthesis.

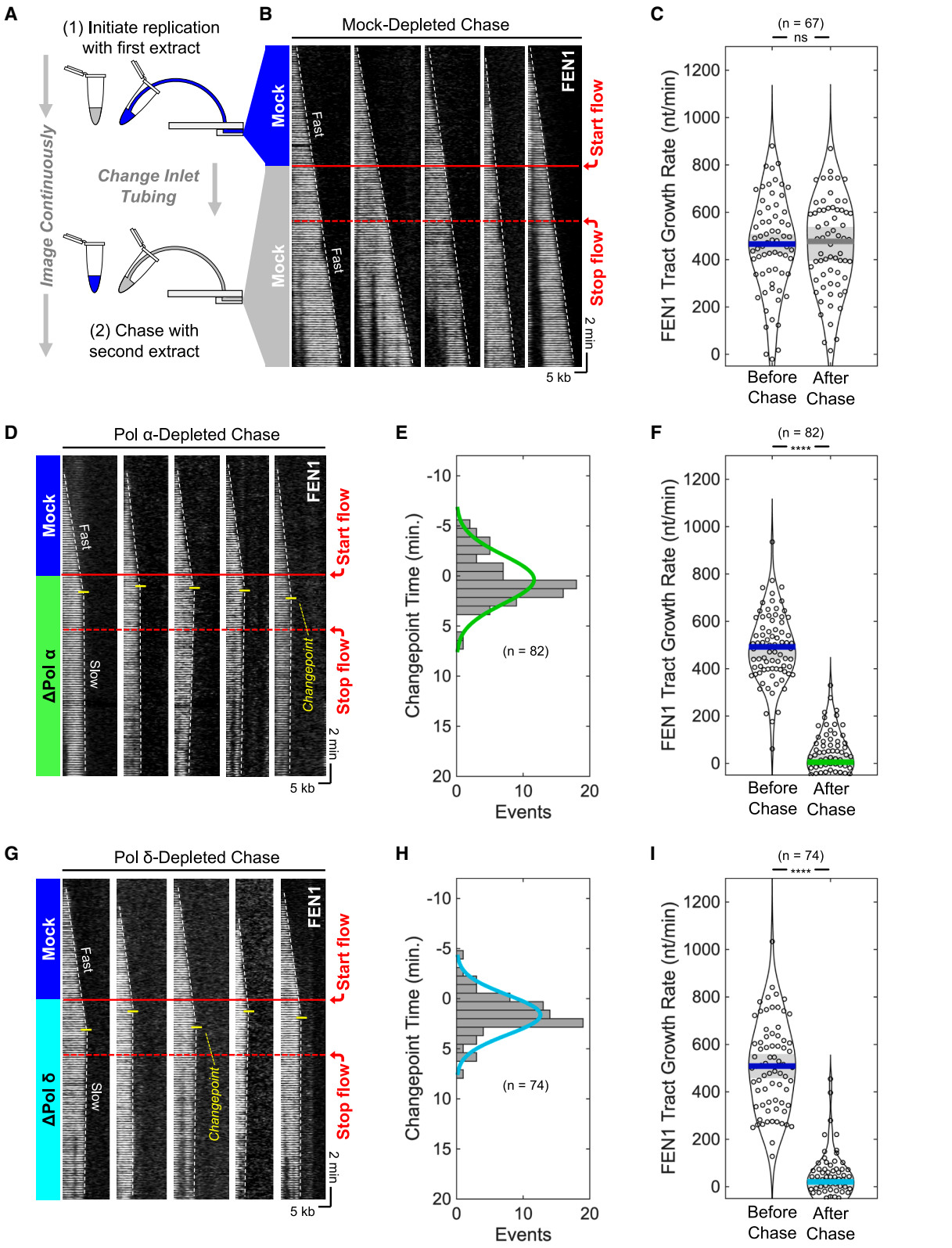
Lagging-strand synthesis stops shortly after chasing with extract depleted of Pol α/δ

The surprisingly short residence time of Pol α/δ on nascent DNA (Figures 1D and 1F) suggests that these polymerases rapidly dissociate from the fork and that new molecules of Pol α/δ are frequently recruited from solution to sustain lagging-strand synthesis. If so, processive lagging-strand synthesis should require an abundant pool of soluble Pol α/δ. To test this hypothesis, we performed a chase experiment in which we initiated replication in undepleted extract, then flushed the flow-cell with mock-depleted, Pol α-depleted, or Pol δ-depleted extract (Figure 3A).

Chasing with mock-depleted extract did not affect the growth of FEN1^{mKikGR} tracts, thus indicating that the chase did not impair lagging-strand synthesis (Figures 3B and 3C). In contrast,

Please cite this article in press as: Lynch et al., Metazoan lagging-strand DNA synthesis is distributive, Cell (2026), https://doi.org/10.1016/j.cell.2026.09.060

CellPress
OPEN ACCESS



(legend on next page)

Please cite this article in press as: Lynch et al., Metazoan lagging-strand DNA synthesis is distributive, Cell (2026), https://doi.org/10.1016/j.cell.2026.09.060

chasing with Pol α-depleted or Pol δ-depleted extract abruptly halted FEN1^{mKikGR} tract growth 1–2 min after starting the chase (Figures 3D–3I). We verified that the chase removed >99% of endogenous Pol α/δ from the flow-cell (Figures S3A and S3B). These experiments indicate that Pol α/δ are not recycled at the fork and that processive lagging-strand synthesis cannot occur in the absence of soluble polymerases. Importantly, this sudden halt in lagging-strand synthesis is not caused by ATR/CHK1 activation, as there is no detectable pCHK1 signal in extract collected from the flow-cell (Figure S3C, lanes 10 and 14), due to the low DNA concentration in these reactions.

We observed similar results when chasing with Pol α/δ-depleted extract supplemented with catalytically dead Pol α/δ (Figures S3D–S3G). These experiments show that neither Pol α nor Pol δ are stably tethered to the replisome, but that new copies of Pol α/δ must be recruited to the fork to support the synthesis of new Okazaki fragments.

Leading- and lagging-strand synthesis are not intrinsically coupled

Our finding that Pol α/δ are not stably affixed to the replisome suggests that leading- and lagging-strand synthesis are not intrinsically coupled. To test this prediction, we performed single-molecule chase experiments in which we monitored single-stranded DNA (ssDNA) accumulation by imaging replication protein A (RPA) tagged with mKikGR (RPA^{mKikGR}) and CMG dynamics by visualizing GINS labeled with Lumidyne555 (GINS^{LD555}).

First, we chased with mock-depleted extract supplemented with DMSO (Figure 4A). During this chase, CMG speed did not change, and there was little RPA^{mKikGR} signal at the fork (Figure 4B) because there is little exposed ssDNA during unperturbed replication.

Second, we chased with mock-depleted extract containing 50 μM of aphidicolin (a replicative polymerase inhibitor that blocks leading- and lagging-strand synthesis[31–33]). During this chase, CMG slowed down to ~40 nt/min and RPA^{mKikGR} accumulated behind the helicase (Figure 4C). This is consistent with previous reports that CMG slows down ~10-fold when DNA synthesis is inhibited,[34] and that fast replisome progression requires leading-strand synthesis by Pol ε.[3]

Third, we chased with extract containing 100 μM of CD437—a Pol α inhibitor.[35] During this chase, a long tract of RPA^{mKikGR} accumulated behind CMG (Figure 4D), which is consistent with RPA binding to the lagging-strand template in the absence of Okazaki fragment synthesis. Notably, CMG did not slow down during the CD437 chase, thus suggesting that blocking Okazaki fragment synthesis did not impair leading-strand synthesis (Figure 4D, cartoon). We verified that nucleotide incorporation continued during the CD437 chase (Figures S4A–S4C). Because 100 μM of CD437 ablates Pol α activity (Figure S4D), any dNTP incorporation must come from leading-strand synthesis.

Finally, we chased with Pol α-depleted extract supplemented with 500 nM of Pol α^{Dead}, which should rapidly block Okazaki fragment synthesis. Like the CD437 chase, chasing with Pol α^{Dead} did not alter CMG speed, but it resulted in massive accumulation of RPA^{mKikGR} behind CMG (Figures 4E and 4F). These data indicate that the rate of leading-strand synthesis is not intrinsically coupled to that of lagging-strand synthesis.

Although lagging-strand priming is suppressed during the Pol α^{Dead} chase, we observed forks where the RPA tract was cleared in the opposite direction of CMG progression (Figure 4G). These events were rare (~1/100 molecules) and likely resulted from infrequent priming by trace amounts of wild-type Pol α remaining after the chase. These RPA-clearing events are consistent with the idea that Pol δ extends Okazaki fragments without being attached to the replisome.

DISCUSSION

Pol α and Pol δ function distributively during lagging-strand synthesis

Data presented here support a distributive mechanism of lagging-strand synthesis in higher eukaryotes (Figure 4H). We find that Pol α resides at the fork long enough for CMG to unwind 150–250 nt of template DNA (Figure 1D), thus indicating that new Pol α molecules must be recruited to prime new Okazaki fragments. We find that Pol δ is deposited behind the fork (Figure 2G), and that lagging strands are extended in the opposite direction of fork progression (Figure 4G), which indicates that Pol δ is not tethered to the replisome. Like Pol α, new Pol δ molecules must be recruited to extend new Okazaki fragments. As CMG continuously unwinds DNA, it exposes the lagging-strand template and facilitates the recruitment of new Pol α/δ molecules for further rounds of distributive Okazaki fragment synthesis.

The distributive mechanism has several potential benefits. (1) It renders lagging-strand replication robust to the binding of inactive Pol α/δ (Figures 2C and 2G). Since Pol α/δ contain Fe-S clusters that are essential for their enzymatic function,[36–38] endogenous or exogenous oxidative stress may inactivate some

Figure 3. Chasing with Pol α/δ-depleted extract rapidly blocks Okazaki fragment synthesis

(A) Diagram of single-molecule chase experiments.
(B) Kymograms of FEN1^{mKikGR} (gray) in a chase experiment with mock-depleted extract. Red lines mark the start/stop of chase flow.
(C) The growth rate of FEN1^{mKikGR} tracts before/after the mock chase.
(D) Kymograms from a chase with Pol α-depleted extract. Dashed line marks the edge of FEN1 tracts fitted by two lines with a changepoint (yellow).
(E) Changepoint time for the chase with Pol α-depleted extract (zero denotes the chase start).
(F) The growth rate of the FEN1^{mKikGR} tracts before/after chasing with Pol α-depleted extract.
(G) Kymograms from a chase with Pol δ-depleted extract.
(H) Changepoint time for the chase with Pol δ-depleted extract.
(I) The growth rate of FEN1^{mKikGR} tracts before/after chasing with Pol δ-depleted extract. In (C), (E), (F), (H), and (I) *n* denotes the number of forks. In (C), (F), and (I), "ns" denotes $p > 0.05$, **** denotes $p < 0.0001$ (computed via Kolmogorov-Smirnov test); boxes represent 95% CI; lines represent the median. In (E) and (H) green/cyan curves represent Gaussian fits.
See also Figure S3.

Please cite this article in press as: Lynch et al., Metazoan lagging-strand DNA synthesis is distributive, Cell (2026), https://doi.org/10.1016/j.cell.2026.09.060

CellPress
OPEN ACCESS

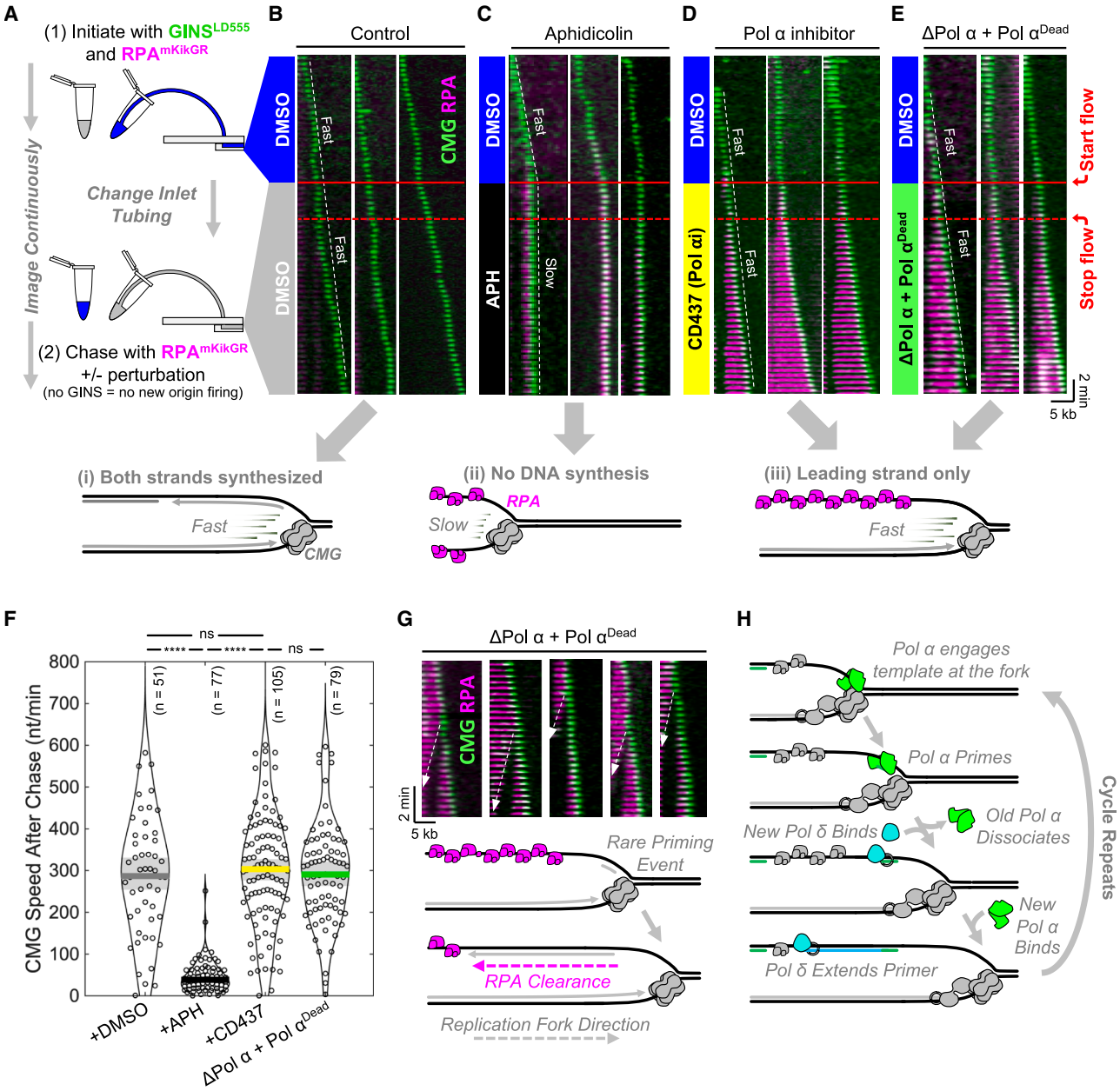


Figure 4. Leading- and lagging-strand synthesis are not intrinsically coupled

(A) Single-molecule chase experiment workflow.

(B) Kymograms of CMG (green) and RPA^{mKikGR} (magenta) where the chase extract contains DMSO. CMG was labeled with GINS^{LD555}.

(C) Kymograms where the chase extract contains 50 μM aphidicolin.

(D) Kymograms where the chase extract contains 100 μM CD437.

(E) Kymograms where the chase contains Pol α-depleted extract with 500 nM Pol α^{Dead}.

(F) CMG speeds measured after the chase. ns denotes $p > 0.05$, **** denotes $p < 0.0001$ (computed via Kolmogorov-Smirnov test). Horizontal lines and boxes represent the median and 95% CI.

(G) Kymograms of CMG (green) and RPA^{mKikGR} (magenta) from experiment in (E) depicting rare events where RPA is cleared away from CMG (cartoon illustrates how RPA is cleared).

(H) Cartoon of proposed distributive mechanism of lagging-strand synthesis.

See also Figure S4.

Please cite this article in press as: Lynch et al., Metazoan lagging-strand DNA synthesis is distributive, Cell (2026), https://doi.org/10.1016/j.cell.2026.09.060

polymerases.[39] (2) It does not require active mechanisms to slow down leading-strand synthesis if it outpaces lagging-strand synthesis. (3) It does not require the lagging-strand template to form loops or any machinery to manage such loops. (4) It may allow replisomes to pass through cohesin rings: CMG alone has a diameter of 10–15 nm,[40] so the persistent presence of Pol α (12–15 nm)[7] and Pol δ (7–10 nm)[41] may impede the ability of the replisome to pass through a cohesin ring (30–40 nm in diameter).[42]

What causes Pol α to dissociate from the replisome? In the absence of nucleotides, Pol α forms a complex with CMG on forked DNA, and this interaction is mediated by multiple CMG-Pol α contacts.[5] Mutating just one of these interfaces destabilizes the CMG-Pol α interaction and reduces priming *in vitro*.[5] We speculate that the major conformational changes experienced by Pol α during primer synthesis[7,8] disrupt Pol α's interaction with CMG, thus triggering its dissociation from the replisome. Future studies capturing CMG-Pol α structures at different stages of primer synthesis are needed to test this prediction.

What causes Pol δ to dissociate from the fork? It could be triggered by Pol δ's low intrinsic processivity, or by its collision with the previous Okazaki fragment.[11] We propose that Pol δ is not tethered to CMG during Okazaki fragment elongation, which is similar to how it functions during homologous recombination[43] and break-induced replication.[44]

Reconciling our observations with previous reports

A study tracking Pol α/δ dynamics in live yeast concluded that these polymerases bind chromatin long enough to synthesize many consecutive Okazaki fragments.[19] However, it remained unclear if the binding events measured in that study occurred at elongating forks. We find that Pol α resides at active forks for only ∼0.5 min compared with > 2 min at stalled forks (Figures S1C and S1D). We surmise that some of the long-lived Pol α binding events reported *in vivo*[19] occurred at stalled forks. Unlike Pol α, we do not observe long-lived Pol δ binding at stalled forks (Figure S1E). It is unclear whether the long-lived binding events measured in yeast[19] reflect Pol δ binding at forks or Pol δ participating in DNA repair.[43–45] In human cells, Pol δ colocalizes with PCNA for only ∼4 s[9] (during which forks travel ∼130 nt in human cells), consistent with the distributive mechanism.

An *in vitro* reconstitution study found that yeast Pol α/δ travel with CMG long enough to synthesize > 100 Okazaki fragments.[18] However, this study used polymerase concentrations 10–100× lower than in cells,[25,46] which cause ATR checkpoint activation in yeast[47,48] and in *Xenopus* nuclear extract (Figures S1J and S1K). We find that Pol α/δ functions distributively across physiological concentrations (Figures 1D and 1F). Interestingly, the same study found that a polymerase-dead but primase-proficient Pol α (equivalent to Pol α^{Dead} used here, Figure 2A) supported DNA replication *in vitro*.[18] This contrasts with our observation that Pol α^{Dead} cannot support replication in extract (Figure 2B). We surmise that RNA primers synthesized by Pol α^{Dead} are unstable in the nucleoplasm (and likely *in vivo*) due to RNases or other enzymes. Contrary to the previous report,[18] we conclude that Pol α's DNA polymerase activity is essential for lagging-strand synthesis.

Previous studies found that decreasing Pol α's concentration *in vitro*[3] or *in vivo*[47] resulted in longer lagging-strand fragments, which is difficult to reconcile with the trombone model. These reports are consistent with the distributive model: low Pol α concentrations cause less frequent priming, resulting in longer Okazaki fragments.

It is possible that discrepancies between our findings and those from yeast studies[18,19] reflect real differences in lagging-strand synthesis mechanisms in fungi versus metazoa. For example, Pol δ's interaction with PCNA is more stable in yeast than in metazoa,[49,50] and yeast Pol δ-PCNA is more processive than its human counterpart.[11,51,52] There are also structural differences in the Pol α-CMG interface between yeast and metazoa.[5] Finally, a recent study reported that Okazaki fragment maturation (which involves the coordinated action of Pol δ and FEN1) is much slower in metazoa than in yeast,[53] which is consistent with our findings that Pol δ does not travel with the fork but remains behind CMG, where it can participate in lagging-strand maturation.

Comparing DNA polymerase dynamics in eukaryotes versus prokaryotes

Classic *in vitro* experiments demonstrated that prokaryotic DNA polymerases can be recycled for multiple Okazaki fragments under dilute conditions, when the recruitment of soluble polymerases is limiting.[16,54,55] However, high processivity under dilute conditions contrasts with lower processivity (i.e., more frequent polymerase exchange) at high concentrations of soluble polymerases.[56–61] To rationalize these discrepancies, a biophysical model was proposed to explain how a protein remains stably associated with a complex at low concentrations, yet it exchanges rapidly with its counterparts in solution at high concentrations.[62] Such concentration-dependent exchange was measured via single-molecule imaging of reconstituted bacterial[61] and yeast[18] replisomes. However, even when polymerases exchange most frequently, individual bacterial DNA polymerases[60,61] or individual yeast Pol α/δ[18] are reused for several consecutive Okazaki fragments.

By contrast, when we recapitulated conditions that should favor polymerase recycling (chasing with polymerase-depleted extract), we did not observe processive Okazaki fragment synthesis (Figures 3D and 3G). This suggests that unlike prokaryotic and fungal systems, metazoan lagging-strand replication is intrinsically non-processive. The need for metazoa to constantly recruit new Pol α/δ molecules during replication may explain why high concentrations of Pol α/δ are present in human cells (∼300–600 nM).[25] For example, there are ∼200,000 copies of Pol α/δ in each human cell,[25] compared with only a few thousand active replication forks at any time.[63,64] This vast excess of lagging-strand DNA polymerases is likely needed to ensure that Pol α/δ are rapidly recruited during Okazaki fragment synthesis.

Leading-strand synthesis and lagging-strand synthesis are not intrinsically coupled

It was previously thought that leading- and lagging-strand synthesis may be intrinsically coordinated to prevent ssDNA accumulation on the lagging-strand template.[65–68] We find that there is no such intrinsic coupling in metazoa (Figure 4F). Instead, our data support a model in which the lagging-strand machinery is rapidly recruited to forks ensuring that Okazaki fragment synthesis keeps up with the rate of leading-strand synthesis. Our

findings are consistent with *in vitro* reconstitution studies reporting that fast leading-strand synthesis can proceed in the absence of lagging-strand synthesis for yeast[3] and human[4] replisomes.

There is conflicting data regarding the coupling of leading- and lagging-strand synthesis in human cells: one study found that treating cells with low doses of the Pol α-inhibitor CD437 does not impair leading-strand synthesis,[69] while another study found that higher doses of CD437 activate ATR and slow down forks, in part via fork reversal.[70] Given that ATR activation is stimulated by primer-template junctions generated by Pol α,[13] it is unclear whether these studies utilized CD437 concentrations sufficient to ablate Pol α activity. Consistent with this idea, another study in human cells found that very high doses of Pol α inhibitor suppress ATR activation.[71] Since there is no checkpoint signaling in our single-molecule experiments (Figure S3C), we demonstrate that metazoan leading- and lagging-strand synthesis are not intrinsically coupled. Such uncoordinated replication was also observed in prokaryotes,[72–74] suggesting a convergent evolution of this mechanism.

Limitations of the study

Immunodepleting Pol δ co-depleted ~90% of Topoisomerase II α (Topo II α), causing a defect in plasmid decatenation (Figures S4E and S4F) that was fully rescued by 200 nM of recombinant Topo II α (Figures S4E and S4G). To mitigate this, we supplemented Pol δ-depleted extract with 200 nM Topo II α in all ensemble experiments.

Pol α's residence time at active forks is consistent with one Pol α molecule priming one Okazaki fragment. We cannot exclude the possibility that occasionally, one Pol α molecule may prime two consecutive Okazaki fragments, as we cannot directly measure individual lagging-strand fragments in our single-molecule assay. We cannot rule out that several Pol δ molecules are needed to extend each Okazaki fragment, as proposed previously.[9]

Except for chase experiments, there is no extract flow during single-molecule experiments. To minimize shear forces, the extract flow rate was kept very low (10 μL/min) during chases, resulting in no distortion of double-tethered DNAs (Figure 3B).

Forks are slower in our experiments (~300–500 nt/min) than in human cells (~1,000–2,000 nt/min) because cells are cultured at 37°C, while our experiments were performed at 24°C (*Xenopus* is a cold-adapted organism and extract experiments fail above ~26°C).

A small fraction (5%–15%) of Pol α/δ-binding events occur behind forks (Figures S4H and S4I)—they may represent polymerases binding to ssDNA gaps far behind CMG or non-specific binding to the coverslip (Figures S4J and S4K).

RESOURCE AVAILABILITY

Lead contact

Requests for further information and resources should be directed to and will be fulfilled by the lead contact, Gheorghe Chistol (chistol@stanford.edu).

Materials availability

Unique reagents generated and described during this study are available upon reasonable request. Some may require a completed materials transfer agreement and compensation for shipping costs.

Data and code availability

- Raw data generated for this study have been deposited to the Stanford Digital Repository and are publicly available at https://doi.org/10.25740/sq803bx0564.
- This paper does not report any original code.
- Any additional information required to reanalyze the data reported in this paper is available from the lead contact upon request.

ACKNOWLEDGMENTS

We thank Karlene Cimprich, Joanna Wysocka, Johannes Walter, David Pellman, Riki Terui, Gongshi Bai, Ulrike Kuehbacher, NaYoung Cheon, Larissa Sambel, Zhitong Feng, and Scott Berger for critiques of the manuscript. We thank Riki Terui for cloning *Xenopus* RPA^{mKikGR}. We thank Johannes Walter for the gift of an initial batch of anti-POLA1 serum. We thank James Dewar for the gift of affinity-purified anti-TOP2A antibodies. We thank Tatsuro Takahashi for the gift of sera against subunits of the FACT complex. We thank Tomasz Swigut for the bioinformatic search of POLD4 in *Xenopus*. L.D.L. was supported by NIH T32GM007276. G.C. is supported by NSF CAREER (2144481), NIGMSR35 (GM147060), and an American Cancer Society seed grant (228425). J.P. is supported by an American Cancer Society award, PF-26-1595977-01-PF MBBW25, with grant DOI https://doi.org/10.53354/ACS.PF-26-1595977-01-PFMBB-W25.pc.gr.246507.

AUTHOR CONTRIBUTIONS

L.D.L. and G.C. conceived the project; L.D.L. carried out all experiments except for those in Figures S4B and S4C, which were carried out by J.P.; J.P. expressed/purified *Xenopus* RPA^{mKikGR} and affinity-purified anti-POLA1 antibodies; G.C. and L.D.L. wrote MATLAB code for data analysis; L.D.L. analyzed all data with input from G.C. and J.P.; L.D.L. and G.C. wrote the manuscript, with input from J.P.

DECLARATION OF INTERESTS

The authors declare no conflicts of interest.

STAR★METHODS

Detailed methods are provided in the online version of this paper and include the following:

- KEY RESOURCES TABLE
- EXPERIMENTAL MODEL AND STUDY PARTICIPANT DETAILS
  - Xenopus Laevis
  - Insect Cell Lines
  - Bacterial Cell Lines Used
- METHOD DETAILS
  - Experimental Design
  - Preparing DNA for Single-Molecule Studies
  - Xenopus Egg Extract Preparation
  - Ensemble Replication Assay
  - Protein Co-Immunoprecipitation Assay
  - Western Blotting and Coomasie Staining
  - Cloning and Plasmids
  - Antibody Preparation
  - Recombinant Protein Expression Purification
  - Fluorescent Labeling Using SFP Synthase
  - Ensemble Plasmid Replication Assay
  - Single Molecule Replication Assay
- QUANTIFICATION AND STATISTICAL ANALYSIS
  - Single-Molecule Data Analysis
  - Selecting DNA Molecules for Analysis
  - Analyzing Polymerase Binding/Dissociation
  - Changepoint Analysis
  - CMG Velocity Analysis
  - Data Reporting

Please cite this article in press as: Lynch et al., Metazoan lagging-strand DNA synthesis is distributive, Cell (2026), https://doi.org/10.1016/j.cell.2026.09.060

- Data Acquisition and Analysis Software
- ADDITIONAL RESOURCES

SUPPLEMENTAL INFORMATION

Supplemental information can be found online at https://doi.org/10.1016/j.cell.2026.09.060.

Received: September 18, 2025
Revised: December 16, 2025
Accepted: September 29, 2026

REFERENCES

1. Nick McElhinny, S.A., Gordenin, D.A., Stith, C.M., Burgers, P.M.J., and Kunkel, T.A. (2008). Division of labor at the eukaryotic replication fork. Mol. Cell *30*, 137–144. https://doi.org/10.1016/j.molcel.2008.02.022.
2. Georgescu, R.E., Langston, L., Yao, N.Y., Yurieva, O., Zhang, D., Finkelstein, J., Agarwal, T., and O'Donnell, M.E. (2014). Mechanism of asymmetric polymerase assembly at the eukaryotic replication fork. Nat. Struct. Mol. Biol. *21*, 664–670. https://doi.org/10.1038/nsmb.2851.
3. Yeeles, J.T.P., Janska, A., Early, A., and Diffley, J.F.X. (2017). How the Eukaryotic Replisome Achieves Rapid and Efficient DNA Replication. Mol. Cell *65*, 105–116. https://doi.org/10.1016/j.molcel.2016.11.017.
4. Baris, Y., Taylor, M.R.G., Aria, V., and Yeeles, J.T.P. (2022). Fast and efficient DNA replication with purified human proteins. Nature *606*, 204–210. https://doi.org/10.1038/s41586-022-04759-1.
5. Jones, M.L., Aria, V., Baris, Y., and Yeeles, J.T.P. (2023). How Pol α-primase is targeted to replisomes to prime eukaryotic DNA replication. Mol. Cell *83*, 2911–2924.e16. https://doi.org/10.1016/j.molcel.2023.06.035.
6. Perera, R.L., Torella, R., Klinge, S., Kilkenny, M.L., Maman, J.D., and Pellegrini, L. (2013). Mechanism for priming DNA synthesis by yeast DNA Polymerase α. eLife *2*, e00482. https://doi.org/10.7554/eLife.00482.
7. Yuan, Z., Georgescu, R., Li, H., and O'Donnell, M.E. (2023). Molecular choreography of primer synthesis by the eukaryotic Pol α-primase. Nat. Commun. *14*, 3697. https://doi.org/10.1038/s41467-023-39441-1.
8. Mullins, E.A., Salay, L.E., Durie, C.L., Bradley, N.P., Jackman, J.E., Ohi, M.D., Chazin, W.J., and Eichman, B.F. (2024). A mechanistic model of primer synthesis from catalytic structures of DNA polymerase α-primase. Nat. Struct. Mol. Biol. *31*, 777–790. https://doi.org/10.1038/s41594-024-01227-4.
9. Drosopoulos, W.C., Vierra, D.A., Kenworthy, C.A., Coleman, R.A., and Schildkraut, C.L. (2020). Dynamic Assembly and Disassembly of the Human DNA Polymerase δ Holoenzyme on the Genome In Vivo. Cell Rep. *30*, 1329–1341.e5. https://doi.org/10.1016/j.celrep.2019.12.101.
10. Bell, S.P., and Labib, K. (2016). Chromosome Duplication in Saccharomyces cerevisiae. Genetics *203*, 1027–1067. https://doi.org/10.1534/genetics.115.186452.
11. Langston, L.D., and O'Donnell, M. (2008). DNA polymerase delta is highly processive with proliferating cell nuclear antigen and undergoes collision release upon completing DNA. J. Biol. Chem. *283*, 29522–29531. https://doi.org/10.1074/jbc.M804488200.
12. Lupardus, P.J., Byun, T., Yee, M.-C., Hekmat-Nejad, M., and Cimprich, K.A. (2002). A requirement for replication in activation of the ATR-dependent DNA damage checkpoint. Genes Dev. *16*, 2327–2332. https://doi.org/10.1101/gad.1013502.
13. MacDougall, C.A., Byun, T.S., Van, C., Yee, M.C., and Cimprich, K.A. (2007). The structural determinants of checkpoint activation. Genes Dev. *21*, 898–903. https://doi.org/10.1101/gad.1522607.
14. Saldivar, J.C., Cortez, D., and Cimprich, K.A. (2017). The essential kinase ATR: ensuring faithful duplication of a challenging genome. Nat. Rev. Mol. Cell Biol. *18*, 622–636. https://doi.org/10.1038/nrm.2017.67.
15. Sinha, N.K., Morris, C.F., and Alberts, B.M. (1980). Efficient in vitro replication of double-stranded DNA templates by a purified T4 bacteriophage replication system. J. Biol. Chem. *255*, 4290–4293. https://doi.org/10.1016/S0021-9258(19)85665-X.
16. Alberts, B.M., Barry, J., Bedinger, P., Formosa, T., Jongeneel, C.V., and Kreuzer, K.N. (1983). Studies on DNA replication in the bacteriophage T4 in vitro system. Cold Spring Harb. Symp. Quant. Biol. *47*, 655–668. https://doi.org/10.1101/sqb.1983.047.01.077.
17. Yao, N.Y., and O'Donnell, M.E. (2016). Evolution of replication machines. Crit. Rev. Biochem. Mol. Biol. *51*, 135–149. https://doi.org/10.3109/10409238.2015.1125845.
18. Lewis, J.S., Spenkelink, L.M., Schauer, G.D., Yurieva, O., Mueller, S.H., Natarajan, V., Kaur, G., Maher, C., Kay, C., O'Donnell, M.E., et al. (2020). Tunability of DNA Polymerase Stability during Eukaryotic DNA Replication. Mol. Cell *77*, 17–25.e5. https://doi.org/10.1016/j.molcel.2019.10.005.
19. Kapadia, N., El-Hajj, Z.W., Zheng, H., Beattie, T.R., Yu, A., and Reyes-Lamothe, R. (2020). Processive Activity of Replicative DNA Polymerases in the Replisome of Live Eukaryotic Cells. Mol. Cell *80*, 114–126.e8. https://doi.org/10.1016/j.molcel.2020.08.014.
20. Walter, J., Sun, L., and Newport, J. (1998). Regulated chromosomal DNA replication in the absence of a nucleus. Mol. Cell *1*, 519–529. https://doi.org/10.1016/S1097-2765(00)80052-0.
21. Hoogenboom, W.S., Klein Douwel, D., and Knipscheer, P. (2017). Xenopus egg extract: A powerful tool to study genome maintenance mechanisms. Dev. Biol. *428*, 300–309. https://doi.org/10.1016/j.ydbio.2017.03.033.
22. Yardimci, H., Loveland, A.B., van Oijen, A.M., and Walter, J.C. (2012). Single-molecule analysis of DNA replication in Xenopus egg extracts. Methods *57*, 179–186. https://doi.org/10.1016/j.ymeth.2012.03.033.
23. Loveland, A.B., Habuchi, S., Walter, J.C., and van Oijen, A.M. (2012). A general approach to break the concentration barrier in single-molecule imaging. Nat. Methods *9*, 987–992. https://doi.org/10.1038/nmeth.2174.
24. Kumamoto, S., Nishiyama, A., Chiba, Y., Miyashita, R., Konishi, C., Azuma, Y., and Nakanishi, M. (2021). HPF1-dependent PARP activation promotes LIG3-XRCC1-mediated backup pathway of Okazaki fragment ligation. Nucleic Acids Res. *49*, 5003–5016. https://doi.org/10.1093/nar/gkab269.
25. Cho, N.H., Cheveralls, K.C., Brunner, A.-D., Kim, K., Michaelis, A.C., Raghavan, P., Kobayashi, H., Savy, L., Li, J.Y., Canaj, H., et al. (2022). OpenCell: Endogenous tagging for the cartography of human cellular organization. Science *375*, eabi6983. https://doi.org/10.1126/science.abi6983.
26. Maga, G., and Hübscher, U. (1996). DNA replication machinery: functional characterization of a complex containing DNA polymerase alpha, DNA polymerase delta, and replication factor C suggests an asymmetric DNA polymerase dimer. Biochemistry *35*, 5764–5777. https://doi.org/10.1021/bi952455k.
27. Schmid, E.W., and Walter, J.C. (2025). Predictomes, a classifier-curated database of AlphaFold-modeled protein-protein interactions. Mol. Cell *85*, 1216–1232.e5. https://doi.org/10.1016/j.molcel.2025.01.034.
28. Yardimci, H., Loveland, A.B., Habuchi, S., van Oijen, A.M., and Walter, J.C. (2010). Uncoupling of sister replisomes during eukaryotic DNA replication. Mol. Cell *40*, 834–840. https://doi.org/10.1016/j.molcel.2010.11.027.
29. Liu, Y., Zhangding, Z., Liu, X., Gan, T., Ai, C., Wu, J., Liang, H., Chen, M., Guo, Y., Lu, R., et al. (2024). Fork coupling directs DNA replication elongation and termination. Science *383*, 1215–1222. https://doi.org/10.1126/science.adj7606.
30. Hu, Z., Perumal, S.K., Yue, H., and Benkovic, S.J. (2012). The human lagging strand DNA polymerase δ holoenzyme is distributive. J. Biol. Chem. *287*, 38442–38448. https://doi.org/10.1074/jbc.M112.404319.
31. Walter, J., and Newport, J. (2000). Initiation of eukaryotic DNA replication: origin unwinding and sequential chromatin association of Cdc45, RPA, and DNA polymerase alpha. Mol. Cell *5*, 617–627. https://doi.org/10.1016/S1097-2765(00)80241-5.
32. Byun, T.S., Pacek, M., Yee, M.C., Walter, J.C., and Cimprich, K.A. (2005). Functional uncoupling of MCM helicase and DNA polymerase activities activates the ATR-dependent checkpoint. Genes Dev. *19*, 1040–1052. https://doi.org/10.1101/gad.1301205.

Please cite this article in press as: Lynch et al., Metazoan lagging-strand DNA synthesis is distributive, Cell (2026), https://doi.org/10.1016/j.cell.2026.09.060

33. Baranovskiy, A.G., Babayeva, N.D., Suwa, Y., Gu, J., Pavlov, Y.I., and Tahirov, T.H. (2014). Structural basis for inhibition of DNA replication by aphidicolin. Nucleic Acids Res. *42*, 14013–14021. https://doi.org/10.1093/nar/gku1209.

34. Sparks, J.L., Chistol, G., Gao, A.O., Räschle, M., Larsen, N.B., Mann, M., Duxin, J.P., and Walter, J.C. (2019). The CMG Helicase Bypasses DNA-Protein Cross-Links to Facilitate Their Repair. Cell *176*, 167–181.e21. https://doi.org/10.1016/j.cell.2018.10.053.

35. Han, T., Goralski, M., Capota, E., Padrick, S.B., Kim, J., Xie, Y., and Nijhawan, D. (2016). The antitumor toxin CD437 is a direct inhibitor of DNA polymerase α. Nat. Chem. Biol. *12*, 511–515. https://doi.org/10.1038/nchembio.2082.

36. Klinge, S., Hirst, J., Maman, J.D., Krude, T., and Pellegrini, L. (2007). An iron-sulfur domain of the eukaryotic primase is essential for RNA primer synthesis. Nat. Struct. Mol. Biol. *14*, 875–877. https://doi.org/10.1038/nsmb1288.

37. Weiner, B.E., Huang, H., Dattilo, B.M., Nilges, M.J., Fanning, E., and Chazin, W.J. (2007). An iron-sulfur cluster in the C-terminal domain of the p58 subunit of human DNA primase. J. Biol. Chem. *282*, 33444–33451. https://doi.org/10.1074/jbc.M705826200.

38. Netz, D.J.A., Stith, C.M., Stümpfig, M., Köpf, G., Vogel, D., Genau, H.M., Stodola, J.L., Lill, R., Burgers, P.M.J., and Pierik, A.J. (2011). Eukaryotic DNA polymerases require an iron-sulfur cluster for the formation of active complexes. Nat. Chem. Biol. *8*, 125–132. https://doi.org/10.1038/nchembio.721.

39. Shaw, A.E., Mihelich, M.N., Whitted, J.E., Reitman, H.J., Timmerman, A.J., Tehseen, M., Hamdan, S.M., and Schauer, G.D. (2024). Revised mechanism of hydroxyurea-induced cell cycle arrest and an improved alternative. Proc. Natl. Acad. Sci. USA. *121*, e2404470121. https://doi.org/10.1073/pnas.2404470121.

40. Yuan, Z., Bai, L., Sun, J., Georgescu, R., Liu, J., O'Donnell, M.E., and Li, H. (2016). Structure of the eukaryotic replicative CMG helicase suggests a pumpjack motion for translocation. Nat. Struct. Mol. Biol. *23*, 217–224. https://doi.org/10.1038/nsmb.3170.

41. Lancey, C., Tehseen, M., Raducanu, V.-S., Rashid, F., Merino, N., Ragan, T.J., Savva, C.G., Zaher, M.S., Shirbini, A., Blanco, F.J., et al. (2020). Structure of the processive human Pol δ holoenzyme. Nat. Commun. *11*, 1109. https://doi.org/10.1038/s41467-020-14898-6.

42. Huis In 't Veld, P.J., Herzog, F., Ladurner, R., Davidson, I.F., Piric, S., Kreidl, E., Bhaskara, V., Aebersold, R., and Peters, J.-M. (2014). Characterization of a DNA exit gate in the human cohesin ring. Science *346*, 968–972. https://doi.org/10.1126/science.1256904.

43. Maloisel, L., Fabre, F., and Gangloff, S. (2008). DNA Polymerase δ Is Preferentially Recruited during Homologous Recombination To Promote Heteroduplex DNA Extension. Mol. Cell. Biol. *28*, 1373–1382. https://doi.org/10.1128/MCB.01651-07.

44. Donnianni, R.A., Zhou, Z.-X., Lujan, S.A., Al-Zain, A., Garcia, V., Glancy, E., Burkholder, A.B., Kunkel, T.A., and Symington, L.S. (2019). DNA Polymerase Delta Synthesizes Both Strands during Break-Induced Replication. Mol. Cell *76*, 371–381.e4. https://doi.org/10.1016/j.molcel.2019.07.033.

45. Meyer, D., Fu, B.X.H., and Heyer, W.-D. (2015). DNA polymerases δ and λ cooperate in repairing double-strand breaks by microhomology-mediated end-joining in Saccharomyces cerevisiae. Proc. Natl. Acad. Sci. USA. *112*, E6907–E6916. https://doi.org/10.1073/pnas.1507833112.

46. Engel, S.R., Aleksander, S., Nash, R.S., Wong, E.D., Weng, S., Miyasato, S.R., Sherlock, G., and Cherry, J.M. (2025). Saccharomyces Genome Database: advances in genome annotation, expanded biochemical pathways, and other key enhancements. Genetics *229*, iyae185. https://doi.org/10.1093/genetics/iyae185.

47. Porcella, S.Y., Koussa, N.C., Tang, C.P., Kramer, D.N., Srivastava, P., and Smith, D.J. (2020). Separable, Ctf4-mediated recruitment of DNA Polymerase α for initiation of DNA synthesis at replication origins and lagging-strand priming during replication elongation. PLoS Genet *16*, e1008755. https://doi.org/10.1371/journal.pgen.1008755.

48. Koussa, N.C., and Smith, D.J. (2021). Limiting DNA polymerase delta alters replication dynamics and leads to a dependence on checkpoint activation and recombination-mediated DNA repair. PLoS Genet. *17*, e1009322. https://doi.org/10.1371/journal.pgen.1009322.

49. Hedglin, M., Pandey, B., and Benkovic, S.J. (2016). Stability of the human polymerase δ holoenzyme and its implications in lagging strand DNA synthesis. Proc. Natl. Acad. Sci. USA. *113*, E1777–E1786. https://doi.org/10.1073/pnas.1523653113.

50. Zheng, F., Georgescu, R.E., Li, H., and O'Donnell, M.E. (2020). Structure of eukaryotic DNA polymerase δ bound to the PCNA clamp while encircling DNA. Proc. Natl. Acad. Sci. USA. *117*, 30344–30353. https://doi.org/10.1073/pnas.2017637117.

51. Podust, V.N., Podust, L.M., Müller, F., and Hübscher, U. (1995). DNA polymerase delta holoenzyme: action on single-stranded DNA and on double-stranded DNA in the presence of replicative DNA helicases. Biochemistry *34*, 5003–5010. https://doi.org/10.1021/bi00015a011.

52. Masuda, Y., Suzuki, M., Piao, J., Gu, Y., Tsurimoto, T., and Kamiya, K. (2007). Dynamics of human replication factors in the elongation phase of DNA replication. Nucleic Acids Res. *35*, 6904–6916. https://doi.org/10.1093/nar/gkm822.

53. Raducanu, V.-S., Tehseen, M., Al-Amodi, A., Joudeh, L.I., De Biasio, A., and Hamdan, S.M. (2022). Mechanistic investigation of human maturation of Okazaki fragments reveals slow kinetics. Nat. Commun. *13*, 6973. https://doi.org/10.1038/s41467-022-34751-2.

54. Wu, C.A., Zechner, E.L., Hughes, A.J., Franden, M.A., McHenry, C.S., and Marians, K.J. (1992). Coordinated leading- and lagging-strand synthesis at the Escherichia coli DNA replication fork. IV. Reconstitution of an asymmetric, dimeric DNA polymerase III holoenzyme. J. Biol. Chem. *267*, 4064–4073. https://doi.org/10.1016/S0021-9258(19)50631-7.

55. Kim, S., Dallmann, H.G., McHenry, C.S., and Marians, K.J. (1996). tau couples the leading- and lagging-strand polymerases at the Escherichia coli DNA replication fork. J. Biol. Chem. *271*, 21406–21412. https://doi.org/10.1074/jbc.271.35.21406.

56. Yang, J., Zhuang, Z., Roccasecca, R.M., Trakselis, M.A., and Benkovic, S.J. (2004). The dynamic processivity of the T4 DNA polymerase during replication. Proc. Natl. Acad. Sci. USA. *101*, 8289–8294. https://doi.org/10.1073/pnas.0402625101.

57. Johnson, D.E., Takahashi, M., Hamdan, S.M., Lee, S.-J., and Richardson, C.C. (2007). Exchange of DNA polymerases at the replication fork of bacteriophage T7. Proc. Natl. Acad. Sci. USA. *104*, 5312–5317. https://doi.org/10.1073/pnas.0701062104.

58. Loparo, J.J., Kulczyk, A.W., Richardson, C.C., and van Oijen, A.M. (2011). Simultaneous single-molecule measurements of phage T7 replisome composition and function reveal the mechanism of polymerase exchange. Proc. Natl. Acad. Sci. USA. *108*, 3584–3589. https://doi.org/10.1073/pnas.1018824108.

59. Liao, Y., Li, Y., Schroeder, J.W., Simmons, L.A., and Biteen, J.S. (2016). Single-Molecule DNA Polymerase Dynamics at a Bacterial Replisome in Live Cells. Biophys. J. *111*, 2562–2569. https://doi.org/10.1016/j.bpj.2016.11.006.

60. Beattie, T.R., Kapadia, N., Nicolas, E., Uphoff, S., Wollman, A.J., Leake, M.C., and Reyes-Lamothe, R. (2017). Frequent exchange of the DNA polymerase during bacterial chromosome replication. eLife *6*, e21763. https://doi.org/10.7554/eLife.21763.

61. Lewis, J.S., Spenkelink, L.M., Jergic, S., Wood, E.A., Monachino, E., Horan, N.P., Duderstadt, K.E., Cox, M.M., Robinson, A., Dixon, N.E., et al. (2017). Single-molecule visualization of fast polymerase turnover in the bacterial replisome. eLife *6*, e23932. https://doi.org/10.7554/eLife.23932.

62. Åberg, C., Duderstadt, K.E., and van Oijen, A.M. (2016). Stability versus exchange: a paradox in DNA replication. Nucleic Acids Res. *44*, 4846–4854. https://doi.org/10.1093/nar/gkw296.

Please cite this article in press as: Lynch et al., Metazoan lagging-strand DNA synthesis is distributive, Cell (2026), https://doi.org/10.1016/j.cell.2026.09.060

63. Cseresnyes, Z., Schwarz, U., and Green, C.M. (2009). Analysis of replication factories in human cells by super-resolution light microscopy. BMC Cell Biol. *10*, 88. https://doi.org/10.1186/1471-2121-10-88.

64. Hawgood, M., Urién, B., Agostinho, A., Thiagarajan, P., Giglio, G., Yang, Y., Zhang, X., Quijada, G., Fonseca, M., Bartek, J., et al. (2025). Spatial mapping of DNA synthesis reveals dynamics and geometry of human replication nanostructures. EMBO J. *44*, 7263–7294. https://doi.org/10.1038/s44318-025-00574-2.

65. Lee, J.-B., Hite, R.K., Hamdan, S.M., Xie, X.S., Richardson, C.C., and van Oijen, A.M. (2006). DNA primase acts as a molecular brake in DNA replication. Nature *439*, 621–624. https://doi.org/10.1038/nature04317.

66. Burgers, P.M.J., and Kunkel, T.A. (2017). Eukaryotic DNA Replication Fork. Annu. Rev. Biochem. *86*, 417–438. https://doi.org/10.1146/annurev-biochem-061516-044709.

67. Gan, H., Yu, C., Devbhandari, S., Sharma, S., Han, J., Chabes, A., Remus, D., and Zhang, Z. (2017). Checkpoint kinase Rad53 couples leading- and lagging-strand DNA synthesis under replication stress. Mol. Cell *68*, 446–455.e3. https://doi.org/10.1016/j.molcel.2017.09.018.

68. Bainbridge, L.J., and Daigaku, Y. (2024). Bulk synthesis and beyond: The roles of eukaryotic replicative DNA polymerases. DNA Repair (Amst) *141*, 103740. https://doi.org/10.1016/j.dnarep.2024.103740.

69. Ercilla, A., Benada, J., Amitash, S., Zonderland, G., Baldi, G., Somyajit, K., Ochs, F., Costanzo, V., Lukas, J., and Toledo, L. (2020). Physiological Tolerance to ssDNA Enables Strand Uncoupling during DNA Replication. Cell Rep. *30*, 2416–2429.e7. https://doi.org/10.1016/j.celrep.2020.01.067.

70. Mehta, K.P.M., Thada, V., Zhao, R., Krishnamoorthy, A., Leser, M., Lindsey Rose, K., and Cortez, D. (2022). CHK1 phosphorylates PRIMPOL to promote replication stress tolerance. Sci. Adv. *8*, eabm0314. https://doi.org/10.1126/sciadv.abm0314.

71. Rodríguez-Acebes, S., Martín-Rufo, R., Gómez-Moya, A., Churcher, S.B., Fernández-Llorente, A., de la Vega-Barranco, G., Perona, A., Oroz, P., Martín-Doncel, E., Toledo, L.I., et al. (2025). DNA polymerase α/primase extraction from chromatin by VCP/p97 restricts ATR activation during unperturbed DNA replication. Nat. Commun. *16*, 5706. https://doi.org/10.1038/s41467-025-60077-w.

72. Graham, J.E., Marians, K.J., and Kowalczykowski, S.C. (2017). Independent and Stochastic Action of DNA Polymerases in the Replisome. Cell *169*, 1201–1213.e17. https://doi.org/10.1016/j.cell.2017.05.041.

73. Marians, K.J. (2018). Lesion Bypass and the Reactivation of Stalled Replication Forks. Annu. Rev. Biochem. *87*, 217–238. https://doi.org/10.1146/annurev-biochem-062917-011921.

74. Stano, N.M., Jeong, Y.-J., Donmez, I., Tummalapalli, P., Levin, M.K., and Patel, S.S. (2005). DNA synthesis provides the driving force to accelerate DNA unwinding by a helicase. Nature *435*, 370–373. https://doi.org/10.1038/nature03615.

75. Berger, S., and Chistol, G. (2024). Visualizing the dynamics of DNA replication and repair at the single-molecule level. Methods Cell Biol. *182*, 109–165. https://doi.org/10.1016/bs.mcb.2023.07.001.

76. Lebofsky, R., Takahashi, T., and Walter, J.C. (2009). DNA replication in nucleus-free Xenopus egg extracts. Methods Mol. Biol. *521*, 229–252. https://doi.org/10.1007/978-1-60327-815-7_13.

77. Weissmann, F., Petzold, G., VanderLinden, R., Huis In 't Veld, P.J., Brown, N.G., Lampert, F., Westermann, S., Stark, H., Schulman, B.A., and Peters, J.-M. (2016). biGBac enables rapid gene assembly for the expression of large multisubunit protein complexes. Proc. Natl. Acad. Sci. USA. *113*, E2564–E2569. https://doi.org/10.1073/pnas.1604935113.

78. Sari, D., Gupta, K., Thimiri Govinda Raj, D.B., Aubert, A., Drncová, P., Garzoni, F., Fitzgerald, D., and Berger, I. (2016). The MultiBac Baculovirus/Insect Cell Expression Vector System for Producing Complex Protein Biologics. Adv. Exp. Med. Biol. *896*, 199–215. https://doi.org/10.1007/978-3-319-27216-0_13.

79. Modesti, M. (2011). Fluorescent labeling of proteins. Methods Mol. Biol. *783*, 101–120. https://doi.org/10.1007/978-1-61779-282-3_6.

80. Yin, J., Straight, P.D., McLoughlin, S.M., Zhou, Z., Lin, A.J., Golan, D.E., Kelleher, N.L., Kolter, R., and Walsh, C.T. (2005). Genetically encoded short peptide tag for versatile protein labeling by Sfp phosphopantetheinyl transferase. Proc. Natl. Acad. Sci. USA. *102*, 15815–15820. https://doi.org/10.1073/pnas.0507705102.

81. Terui, R., Berger, S.E., Sambel, L.A., Song, D., and Chistol, G. (2024). Single-molecule imaging reveals the mechanism of bidirectional replication initiation in metazoa. Cell *187*, 3992–4009.e25. https://doi.org/10.1016/j.cell.2024.05.024.

82. Cavanaugh, J.E., and Neath, A.A. (2019). The Akaike information criterion: Background, derivation, properties, application, interpretation, and refinementsapplication. WIREs Comput. Stat. *11*, e1460. https://doi.org/10.1002/wics.1460.

Please cite this article in press as: Lynch et al., Metazoan lagging-strand DNA synthesis is distributive, Cell (2026), https://doi.org/10.1016/j.cell.2026.09.060

CellPress
OPEN ACCESS

STAR★METHODS

KEY RESOURCES TABLE

REAGENT or RESOURCE	SOURCE	IDENTIFIER
Antibodies		
Rabbit Anti-xPOLA1	This paper	N/A
Rabbit Anti-xPOLD1	This paper	N/A
Rabbit Anti-xGINS	Terui et al.[81]	N/A
Peroxidase AffiniPure Rabbit Anti-Mouse IgG (H + L)	Jackson Immuno Research Labs	Cat# 315-035-003; RRID:AB_2340061
Bacterial and virus strains		
DH5α	NEB	Cat# C2987H
DH10EMBacY	Geneva Biotech	Cat# DH10EMBacY
Rosetta (DE3) pLysS	Novagen	Cat# 70956-4
Chemicals, peptides, and recombinant proteins		
BamHI-HF	NEB	Cat# R3136S
BstXI	NEB	Cat# R0113S
HindIII-HF	NEB	Cat# R3104S
NcoI-HF	NEB	Cat# R3193S
NotI-HF	NEB	Cat# R3189S
SalI-HF	NEB	Cat# R3138S
SwaI	NEB	Cat# R0604S
PI-SceI	NEB	Cat# R0696S
PmeI	NEB	Cat# R0560S
XhoI	NEB	Cat# R0146S
Klenow Fragment (3′–5′ exo-) polymerase	NEB	Cat# M0212S
Proteinase K	NEB	Cat# P8107S
[α-32P] dCTP	PerkinElmer	Cat# BLU513A250UC
biotin-dCTP	Thermo Fisher Scientific	Cat# 19518018
biotin-dGTP	PerkinElmer	Cat# NEL541001EA
L-Cysteine hydrochloride monohydrate	Fisher Scientific	Cat# ICN10144601
Cycloheximide	Sigma Aldrich	Cat# 01810
Aprotinin	Sigma Aldrich	Cat# 11583794001
Leupeptin	Sigma Aldrich	Cat# 11529048001
Cytochalasin B from Drechslera dematioidea	Sigma Aldrich	Cat# C6762
Dithiothreitol (DTT)	Bio-Rad	Cat# 1610611
Nocodazole	Sigma Aldrich	Cat# M1404
Dimethyl sulfoxide (DMSO)	Sigma Aldrich	Cat# D8418
Adenosine 5′-triphosphate disodium salt hydrate (ATP)	Sigma Aldrich	Cat# A7699
Phosphocreatine disodium salt hydrate (PC)	Sigma Aldrich	Cat# P7956
Creatine Phosphokinase from rabbit muscle (CPK)	Sigma Aldrich	C3755
FEN1mkikGR	Terui et al.[81]	N/A
His6-Human Rhinovirus (HRV) 3C Protease	Terui et al.[81]	N/A
Alexa Fluor 647 C2 Maleimide	Thermo Fisher Scientific	Cat# A20347
Lumidyne 555 CoA Conjugate	Lumidyne Technologies	Custom Quote
Lumidyne 655 CoA Conjugate	Lumidyne Technologies	Custom Quote

(*Continued on next page*)

Please cite this article in press as: Lynch et al., Metazoan lagging-strand DNA synthesis is distributive, Cell (2026), https://doi.org/10.1016/j.cell.2026.09.060

Continued

REAGENT or RESOURCE	SOURCE	IDENTIFIER
Ni-NTA Agarose	Qiagen	Cat# 30230
Imidazole	Fisher Scientific	Cat# 03196-500
Dynabeads Protein A	Invitrogen	Cat# 10002D
rProtein A Sepharose Fast Flow	GE Healthcare	Cat# 171279
AminoLink Plus Coupling Resin	Fisher Scientific	Cat# PI20501
Cellfectin II Reagent	Fisher Scientific	Cat# 10-362-100
LB Broth	Thermo Fisher Scientific	Cat# BP9723
LB Agar	Thermo Fisher Scientific	Cat# BP9724
ESF 921 Insect Cell Culture Medium, Protein Free	Expression Systems	Cat# 96-001-01
Superdex 200 Increase 10/300 GL	Cytiva	Cat# 28990944
Mono Q 5/50 GL	Cytiva	Cat# 17516601
Mono S 5/50 GL	Cytiva	Cat# 17516801
Amicon Ultra-4-10K	Merck Millipore	Cat# UFC801024
Spectrum Spectra/Por 1 RC Dialysis Membrane Tubing 6–8 kD	Spectrum Labs	Cat# 132645
Spectrum Spectra/Por 4 RC Dialysis Membrane Tubing 12–14 kD	Spectrum Labs	Cat# 132700
Pierce Protease Inhibitor Tablets, EDTA-free	ThermoFisher Scientific	Cat# A32965
4%–15% Mini-PROTEAN TGX Precast Protein Gels	Bio-Rad	Cat# 4561086
Tris-Glycine-SDS Running Buffer	Boston BioProducts	Cat# BP-150
EZ-Run Prestained Rec Protein Ladder	Fisher Scientific	Cat# BP36031
Precision Plus Protein Dual Color Standard	Bio-Rad	Cat# 1610374EDU
SuperSignal West Pico PLUS Chemiluminescent Substrate	Fisher Scientific	Cat# PI34577
Optiblot Blue InstantBlue Coomassie Protein Stain	Abcam	Cat# ab119211
PVDF membranes	VWR	Cat# 10061-492
Transfer Buffer	Fisher Scientific	Cat# NC9297917
Phosphate Buffered Saline (10x, pH 7.4)	Fisher Scientific	Cat# NC9140736
CHORULON Hormone	Merck	Cat# 133754
75 × 25 × 1 mm Glass Slides	VWR	Cat# 48300-026
High Precision Glass CoverSlip, No 1.5, 24 × 60 mm	Bioscience Tools	Cat# CSHP-No1.5-24x60
Double-sided tape	Grace Bio-Labs	SKU 62001
mPEG-Succinimidyl Valerate, MW 5,000	Laysan Bio	Cat# MPEG-SVA-5000-1g
Biotin-PEG-SVA, MW 5,000	Laysan Bio	Cat# Biotin-PEG-SVA-5000-100MG
Streptavidin from Streptomyces avidinii	Sigma Aldrich	Cat# S4762-5MG
Streptavidin, Alexa Fluor 647 conjugate	Thermo Fisher Scientific	Cat# S21374
Aphidicolin from Nigrospora sphaerica	Sigma-Aldrich	Cat# A0781-5MG
Critical commercial assays		
Q5 High-Fidelity 2X Master Mix	NEB	Cat# M0492S
NEBuilder HiFi DNA Assembly Master Kit	NEB	Cat# E2621S
ZR BAC DNA Miniprep kit	Zymo Research	Cat# D4049
Deposited data		
Raw data from this paper	Stanford Digital Repository	https://doi.org/10.25740/sq803bx0564
Experimental models: Cell lines		
Sf9 insect cells	Expression Systems	Cat# 94-001S

(*Continued on next page*)

Please cite this article in press as: Lynch et al., Metazoan lagging-strand DNA synthesis is distributive, Cell (2026), https://doi.org/10.1016/j.cell.2026.09.060

Continued

REAGENT or RESOURCE	SOURCE	IDENTIFIER
Tni insect cells	Expression Systems	Cat# 94-002S
Experimental models: Organisms/strains		
Xenopus laevis, adult female	Nasco Healthcare	Cat# LM00531; RRID:XEP_Xla
Xenopus laevis, adult male	Nasco Healthcare	Cat# LM00715MX
Oligonucleotides		
Forward cDNA primer for pola1.S: atgtcagactccggaagtttcg	This paper	N/A
Reverse cDNA primer for pola1.S: ttatttaatggtgttgagtgtctggaacagct	This paper	N/A
Forward cDNA primer for pola2.L: atgtctgtgtcagcaaagagcatt	This paper	N/A
Reverse cDNA primer for pola2.L: ttaaactctcaccacctgagcagaa	This paper	N/A
Forward cDNA primer for prim1.S: atggatttgtcggtgtatgatccg	This paper	N/A
Reverse cDNA primer for prim1.S: ttaaaattctttcttcagatcacttttgttcagaagt	This paper	N/A
Forward cDNA primer for prim2.S: atgctgttctccagggatagaaaatatagg	This paper	N/A
Reverse cDNA primer for prim2.S: tcagtattcactgaagatctgctctagg	This paper	N/A
Forward cDNA primer for pold1.L: atggatttcaaaagaaagaaaggaccatct	This paper	N/A
Reverse cDNA primer for pold1.L: ccaagctgggggtccaaag	This paper	N/A
Forward cDNA primer for pold2.L: atgtttacagatctagctatttctggggg	This paper	N/A
Reverse cDNA primer for pold2.L: tcaatcacccaattcgtcatctgc	This paper	N/A
Forward cDNA primer for pold3.L: atggacgagctgtacctggag	This paper	N/A
Reverse cDNA primer for pold3.L: tcacttcttctggaagaagcccat	This paper	N/A
Forward cDNA primer for top2a.L: atggagaccgaacctttgcagc	This paper	N/A
Reverse cDNA primer for top2a.S: ttaaaagtcatcgtcagaatcctccag	This paper	N/A
Recombinant DNA		
pJP006: Pol α antigen (POLA1; Amino acids 1 – 340-6xHis)	This paper	N/A
pLDL048: Pol δ antigen (POLD1; Amino Acids 1 – 89 -6xHis)	This paper	N/A
pLDL113: GINS-S6-6xHis	This paper	N/A
pLDL157: TwinStrep-HRV3C-S6-Pol α	This paper	N/A
pLDL158: TwinStrep-HRV3C-S6-Pol δ	This paper	N/A
pLDL171: TwinStrep-HRV3C-S6-Pol αDead (POLA1; D998S and D1000S)	This paper	N/A
pLDL184: TwinStrep-HRV3C-S6-Pol δDead (POLD1; D606A and D761A)	This paper	N/A
pLDL189: Twinstrep-HRV3C-Topoisomerase II α	This paper	N/A

(*Continued on next page*)

Please cite this article in press as: Lynch et al., Metazoan lagging-strand DNA synthesis is distributive, Cell (2026), https://doi.org/10.1016/j.cell.2026.09.060

Continued

REAGENT or RESOURCE	SOURCE	IDENTIFIER
Software and algorithms		
MATLAB	Mathworks	matlab; RRID:SCR_001622
ImageJ	NIH	imagej; RRID:SCR_003070
Image Stabilizer Plugin for ImageJ	Kang Li	https://www.cs.cmu.edu/~kangli/code/Image_Stabilizer.html

EXPERIMENTAL MODEL AND STUDY PARTICIPANT DETAILS

Xenopus Laevis

Eggs from adult (2–4 years old), female *Xenopus laevis* frogs (RRID:XEP_Xla, NASCO Healthcare, Cat# LM00531) were used to prepare egg extracts and the testes of adult, male *Xenopus laevis* frogs (NASCO Healthcare, Cat# LM00715MX) were used to prepare sperm chromatin. All animals were healthy, not subjected to previous procedures, and no animal husbandry was performed. Frogs were housed at the Boswell Small Amphibians Research Facility at Stanford School of Medicine in compliance with Institute Animal Care and Use Committee (IACUC) regulations and all experiments involving frogs were approved by the Stanford University APLAC (Administrative Panel on Laboratory Animal Care).

Insect Cell Lines

Sf9 cells (Expression Systems, Cat# 94-001S) and Tni cells (Expression Systems, Cat# 94-002S) were cultured in ESF 921 insect cell culture medium (Expression Systems, Cat# 96-001-01) at 27°C for baculovirus production and protein overexpression.

Bacterial Cell Lines Used

DH10EMBacY (Geneva Biotech, Cat# DH10EMBacY), DH5α (New England Biolabs (NEB), Cat# C2987H), and Rosetta (DE3) pLysS (Novagen, Cat# 70956-4) bacteria were cultured in LB broth (Thermo Fisher Scientific, Cat# BP9723) at 37C for plasmid production and protein overexpression.

METHOD DETAILS

Experimental Design

Each experiment was repeated at least twice, with independent extract preparations. No randomization/stratification strategy was used. At least 50–100 individual measurements (replication forks, polymerase binding events, etc.) were used for quantification (the exact number is reported in each figure, with details in the figure legend).

Preparing DNA for Single-Molecule Studies

All single molecule experiments used doubly tethered λ phage DNA. The 48.5 kb DNA substrate as purchased from NEB (#N3011S) has 12-nt 5′ ssDNA overhangs on both ends. We used the Klenow Fragment (3′ to 5′ exo-) polymerase (NEB, Cat# M0212S) to fill in the overhangs with biotin-dCTP (Thermo Fisher Scientific, Cat# 19518018) and biotin-dGTP (PerkinElmer, Cat# NEL541001EA). The product is separated with electrophoresis and electro-eluted from the gel before use in tethering. A step-by-step detailed protocol for preparing biotinylated λ DNA is available in.[75]

Xenopus Egg Extract Preparation

Xenopus laevis egg extracts were prepared following published protocols.[34,76] Frogs were primed with 50 IU of human chorionic gonadotropin (CHORULON) (Merck, Cat# 133754) 5–7 days before extract preparation. To induce ovulation, 500 IU of CHORULON was injected 20–22 hr before extract preparation. High-speed supernatant (HSS) was prepared from 5–6 adult female frogs, and nucleoplasmic extract (NPE) was prepared from 15–20 frogs. Sperm chromatin was purified from adult male frog testes and used for NPE preparation.

Ensemble Replication Assay

To validate antibodies and recombinant proteins, ensemble DNA replication experiments were performed following a detailed protocol described in a recent methods article.[75] Since all proteins of interest (POIs) in this study are dispensable for Mcm2-7 double-hexamer loading, all licensing reactions were performed with HSS depleted of POI.

Protein Co-Immunoprecipitation Assay

To test if Pol α and Pol δ form a complex in solution, 100 nM of each polymerase was mixed together in a 20 μL reaction made up of ELB-Sucrose, 0.05% NP-40S, and 0.1 mg/mL BSA. The mixture was incubated for 1 hour at room-temperature with gentle rotation. 10 μg of affinity-purified anti-POLD1 antibody was incubated with 60 μg Dynabeads Protein A (Invitrogen, Cat# 10002D) for 1 hour at

Please cite this article in press as: Lynch et al., Metazoan lagging-strand DNA synthesis is distributive, Cell (2026), https://doi.org/10.1016/j.cell.2026.09.060

room-temperature with gentle rotation. Beads were washed twice with ELB-Sucrose + 0.05% NP-40S and then incubated with the polymerase mixture and incubated for 1 hour at room-temperature with gentle rotation. Beads were washed three times with ice-cold ELB-Sucrose + 0.05% NP-40S. Bound proteins were eluted by boiling beads in 15 μL 1x Laemmli buffer (50mM Tris-HCl pH 6.8, 2% SDS, 10% glycerol, 0.1% bromophenol blue, 2.5% β-mercaptoethanol).

Western Blotting and Coomasie Staining

All samples were boiled in 1x Laemmli buffer and run on 4%–15% Mini-PROTEAN TGX Precast Protein Gels (Bio-Rad #4561086) using Tris-Glycine-SDS Running Buffer (Boston BioProducts #BP-150). EZ-Run Prestained Rec Protein Ladder (Fisher Scientific #BP36031) or Precision Plus Protein Dual Color Standard (Bio-Rad #1610374EDU) was run alongside samples to infer protein band sizes. For Coomasie staining, protein gels were incubated with Optiblot Blue InstantBlue Coomassie Protein Stain (Abcam #ab119211) for at least 1 hour at room temperature with gentle shaking. For immunoblotting, proteins were transferred from the gel onto a PVDF membrane (VWR #10061-492) in transfer buffer (Fisher Scientific #NC9297917). Membranes were blocked in 1x TBST (1x Tris Buffered Saline (TBS) (25 mM Tris pH 7.4, 150 mM NaCl), 0.1% Tween 20) containing 5% (w/v) BSA for 1 hour at room temperature with gentle shaking. Following a wash in 1xTBST, the membrane was incubated with primary antibodies diluted in 1x TBST containing 5% (w/v) BSA overnight at 4C with gentle shaking. Membranes were washed three times with 1x TBST and incubated with secondary antibody diluted in 1x TBST + 5% BSA for 1 hour at room temperature with gentle shaking. Membranes were washed three times with 1x TBST, developed using SuperSignal West Pico PLUS Chemiluminescent Substrate (Fisher Scientific, Cat# PI34577), and imaged using Azure c600 (Azure Biosystems).

Cloning and Plasmids

To prepare an antigen consisting of *Xenopus laevis* POLA1 amino acids 1 – 340, the corresponding DNA sequence was PCR amplified out of *X. laevis* egg cDNA. The resulting PCR product was assembled into pET28b(+) using the NEBuilder HiFi Mix (NEB, Cat# E2621S), yielding plasmid pJP006.

To prepare an antigen consisting of *X. laevis* POLD1 amino acids 1 – 89, the corresponding DNA sequence was PCR amplified out of *X. laevis* egg cDNA. The resulting PCR product was assembled into pET28b(+) using the NEBuilder HiFi Mix (NEB, cat# E2621S), yielding plasmid pLDL048.

To prepare full-length *X. laevis* Pol α individual subunits were first cloned out of cDNA. The *pola1* gene was PCR amplified out of cDNA and assembled into BamHI/HindIII linearized pLib, yielding plasmid pLDL152. The *pola2* gene was PCR amplified out of cDNA and assembled into BamHI/HindIII linearized pLib, yielding plasmid pLDL153. The *prim1* gene was PCR amplified out of cDNA using primers and assembled into BamHI/HindIII linearized pLib, yielding plasmid pLDL154. The *prim2* gene was PCR amplified out of cDNA and assembled into BamHI/HindIII linearized pLib, yielding plasmid pLDL155. To tag the N-terminus of POLA1 with a TwinStrep-3aaLinker-HRV3C-S6-10aaLinker cassette, the *pola1* gene was PCR amplified out of pLDL152 and the resulting PCR product was assembled with a geneblock (synthesized by IDT) into BamHI/HindIII linearized pLib yielding plasmid pLDL156. All four subunits were then cloned into a single plasmid using the biGBac multigene construction strategy.[77] *twinstrep-3aalinker-hrv3c-s6-10aalinker-pola1* was PCR amplified out of LDL156 using primers oLDL108/oLDL109, *pola2* was PCR amplified out of pLDL153 using primers oLDL110/oLDL111, *prim1* was PCR amplified out of pLDL154 using primers oLDL112/oLDL113, and *prim2* was PCR amplified out of pLDL155 using primers oLDL114/oLDL117. The four resulting PCR products were assembled into SwaI linearized pBiG1a, yielding the complete insect expression plasmid pLDL157.

To prepare a polymerase dead *X. laevis* Pol α, essential aspartic acids in the DNA polymerase active site of POLA1 were mutated to serine as previously described for the *Saccharomyces cerevisiae* ortholog.[18] D996 and D998 from *S. cerevisiae* Pol1 were mapped to D998 and D1000 in *X. laevis* POLA1.

To prepare full-length *X. laevis* Pol δ individual subunits were first cloned out of cDNA. The *pold1* gene was PCR amplified out of cDNA and assembled with a *3xflag-3aalinker-hrv3c-s6-10aalinker* containing geneblock (synthesized by IDT) into pACEBac1, yielding plasmid pLDL148. The *pold2* gene was PCR amplified out of cDNA and assembled into pIDC, yielding plasmid pLDL079. The *pold3* gene was PCR amplified out of cDNA using primers and assembled into pIDC, yielding plasmid pLDL080. All three subunits were then cloned into a single plasmid using the MultiBac multigene construction strategy.[78] The *pold3* gene was extracted from pLDL080 and inserted into linearized pLDL079, yielding pLDL081. The pLDL081 and pLDL148 vectors were fused by Cre-recombination, yielding pLDL149. The 3xFLAG tag was replaced by a TwinStrep tag via Gibson assembly, yielding the complete insect expression plasmid pLDL158.

To prepare a polymerase dead *X. laevis* Pol δ, essential aspartic acids in the DNA polymerase active site of POLD1 were mutated to alanine as previously described for the *Homo sapiens* ortholog.[9] D602 and D757 from *H. sapiens* POLD1 were mapped to D606 and D761 in *X. laevis* POLD1.

To prepare full- length *X. laevis* Topo II α the gene for *top2a* was cloned out of cDNA and inserted into a PCR linearized pLib backbone that already contained the DNA sequence for an upstream *twinstrep-HRV3C* cassette, yielding the insect expression plasmid pLDL189.

To prepare full-length *X. laevis* GINS with an S6 tag, a pGC124 containing *psf3-10aaLinker-sort-6xhis* and *sld5* was used as a starting point. A *10aalinker-s6-6xhis* cassette was added to the C-terminus of *psf3*, yielding the *psf3-10aaLinker-s6-6xhis* and *sld5* containing plasmid pLDL112. The pLDL112 (psf3-*10aaLinker-s6-6xhis*/*sld5*) and pGC033 (*psf1*/*psf2*) vectors were fused by Cre-recombination, yielding the complete GINS expression plasmid pLDL113.

Please cite this article in press as: Lynch et al., Metazoan lagging-strand DNA synthesis is distributive, Cell (2026), https://doi.org/10.1016/j.cell.2026.09.060

Antibody Preparation

Custom polyclonal antibodies were generated as previously described.[75] Briefly, the His6 tagged antigen sequence was cloned into pET28b(+) (see Cloning and Plasmids). The antigen was expressed in Rosetta (DE3) pLysS (Novagen, Cat# 70956-4) upon induction with 0.5–1.0 mM IPTG for 3 hrs at 37°C. Soluble antigens were purified in native buffer, whereas insoluble antigens were purified in denaturing buffer (see table and 'Recombinant Protein Expression and Purification' below). The Ni-NTA eluate (still containing 400 mM imidazole) was used to immunize rabbits. All antibodies used in this study were raised by Cocalico Biologicals.

All antibodies used in this study were affinity purified. 1–5 mg of purified antigen was cross-linked to 1 mL of AminoLink Plus Coupling Resin (Fisher Scientific, Cat# PI20501) according to the manufacturer's protocol. 10–30 mL of serum was incubated with the affinity resin for 30 minutes at room temperature. The resin was washed twice with 10 mL of 1x PBS + 500 mM NaCl, and twice again with 10 mL of 1x PBS. Next, antibodies bound to the affinity resin were eluted 5–6 times with 1.0 mL of 200 mM glycine-HCl pH2.5. Each elution was collected into a tube containing 0.1 mL of 1M Tris-HCl pH 9.0, which immediately neutralized the glycine. Eluted fractions were pooled and dialyzed against 1 L of 1x TBS (50 mM Tris-HCl pH8.0, 150 mM NaCl) + 10% (w/v) sucrose. The IgG concentration was measured using a Nanodrop, normalized to 1 mg/mL via dilution or spin-concentration, aliquots were flash frozen in liquid nitrogen, and stored at -80°C.

Target protein (Rabbit #)	Antigen	Plasmid	Antigen purification	Depletion Condition μg IgG per μL extract	Primary Ab. Conc. for WB
Anti-xGINS, (SU289)	Whole GINS complex Psf2-10aa-sort-His6	pGC127, (insect)	Native	1:1	0.2 μg/mL
Anti-xPOLA1 (SU375)	(1–340 aa)-His6	pJP006 (bacteria)	Native	2:1	0.2 μg/mL
Anti-xPOLD1, (SU329)	(1–89 aa)-His6	pLDL048 (bacteria)	Native	1:1	0.2 μg/mL

Recombinant Protein Expression Purification

FEN1^{mKikGR}, RPA^{mKikGR}, and SFP Synthase were purified following previously published protocols.[23,79,80]

Pol α was purified as follows. A bacmid was generated by transforming DH10EMBacY cells with [pLDL157] pBiG_TwinStrep-HRV3C-S6-Pol α, and the resulting bacmid was purified with the ZR BAC DNA Miniprep Kit (Zymo Research, Cat# D4049). Baculovirus was amplified in three 72-hour stages (P0, P1, P2) in Sf9 cells. TwinStrep-HRV3C-S6-Pol α was expressed in 1 L of Tni suspension culture by infection with 2 mL of P2 baculovirus for 48 hrs. Cells were harvested, pelleted by centrifugation, and flash frozen in liquid nitrogen. Cell pellets were thawed and resuspended in 100 mL of lysis buffer (25 mM HEPES-NaOH pH 7.5, 300 mM NaCl, 10% glycerol, 1 mM DTT – bubbled with argon gas to remove dissolved oxygen) supplemented with 1x Pierce Protease Inhibitor EDTA-free (ThermoFisher Scientific, Cat# A32965) and lysed by Dounce homogenization. Lysate was cleared by ultracentrifugation at 35,000 rpm for 45 min at 4°C in a Beckman Type 70 Ti rotor (Beckman Coulter). Cleared lysate was incubated with 1 mL of Strep-Tactin®XT 4®Flow resin (IBA Lifesciences, Cat# 2-5010-010) for 1 hr at 4°C. The resin was washed with 3x10 mL lysis buffer. The protein was eluted from the resin using 4 mL lysis buffer supplemented with 50 μg/mL HRV3C Protease for 2 hours at 4°C on a rotator, and flash frozen in liquid nitrogen. Eluent was thawed and, diluted with 2 mL of no-salt buffer (25 mM HEPES-NaOH pH 7.5, 10% glycerol, 1 mM DTT) to reduce the NaCl concentration to 200 mM, and loaded on a Mono Q 5/50 GL column (Cytiva, Cat# 17516601). The protein was eluted in 20 CVs off the column with a linear gradient of 200 mM – 1000 mM NaCl and eluted around ~400 mM NaCl. Peak fractions were pooled, spin concentrated to ~0.5 mL using the Amicon Ultra-4-10K column (Merck Millipore, Cat# UFC801024) applied to a Superdex 200 Increase 10/300 gel-filtration column (Cytiva, Cat# 28-9909-44) equilibrated in 25 mM HEPES-NaOH pH 7.5, 10% glycerol, 1 mM DTT and 150 mM NaCl. Peak fractions were pooled, spin concentrated to ~6 μM using the Amicon Ultra-4-10K column (Merck Millipore, Cat# UFC801024), and frozen in liquid nitrogen and stored at −80 °C. Approximately 100 μg total protein was obtained from 1 L of Tni cells. The Pol α^{Dead} mutant was purified as described for the wild-type protein.

Pol δ was purified as follows. A bacmid was generated by transforming DH10EMBacY cells with [pLDL158] pBiG_TwinStrep-HRV3C-S6-Pol δ, and the resulting bacmid was purified with the ZR BAC DNA Miniprep Kit (Zymo Research, Cat# D4049). Baculovirus was amplified in three 72-hour stages (P0, P1, P2) in Sf9 cells. We initially attempted to express Pol δ in Tni Cells, however the POLD3 subunit was not recovered (presumably due to proteolysis). Instead, TwinStrep-HRV3C-S6-Pol δ was expressed in 2 L of Sf9 suspension culture by infection with 4 mL of P2 baculovirus for 65 hrs. Cells were harvested, pelleted by centrifugation, and flash frozen in liquid nitrogen. Cell pellets were thawed and resuspended in 200 mL of lysis buffer (25 mM HEPES-NaOH pH 7.5, 300 mM NaCl, 10% glycerol, 1 mM DTT – bubbled with argon gas to remove dissolved oxygen) supplemented with 1x Pierce Protease Inhibitor EDTA-free (ThermoFisher Scientific, Cat# A32965) and lysed by Dounce homogenization. Lysate was cleared by ultracentrifugation at 35,000 rpm for 45 min at 4°C in a Beckman Type 70 Ti rotor (Beckman Coulter). Cleared lysate was incubated with 1 mL of Strep-Tactin®XT 4®Flow resin (IBA Lifesciences, Cat# 2-5010-010) for 1 hr at 4°C. The resin was washed with 3x10mL lysis buffer. The protein was eluted from the resin using 4 mL lysis buffer supplemented with 50 μg/mL HRV3C Protease for 2 hours at 4°C

Please cite this article in press as: Lynch et al., Metazoan lagging-strand DNA synthesis is distributive, Cell (2026), https://doi.org/10.1016/j.cell.2026.09.060

on a rotator, and flash frozen in liquid nitrogen. Eluent was thawed and, diluted with 2 mL of no-salt buffer (25 mM HEPES-NaOH pH 7.5, 10% glycerol, 1 mM DTT) to reduce the NaCl concentration to 200 mM, and loaded on a Mono Q 5/50 GL column (Cytiva, Cat# 17516601). The protein was eluted in 20 CVs off the column with a linear gradient of 200 mM – 1000 mM NaCl and eluted around ~350 mM NaCl. Peak fractions were pooled, spin concentrated to ~0.5 mL using the Amicon Ultra-4-10K column (Merck Millipore, Cat# UFC801024) applied to a Superdex 200 Increase 10/300 gel-filtration column (Cytiva, Cat# 28-9909-44) equilibrated in 25 mM HEPES-NaOH pH 7.5, 10% glycerol, 1 mM DTT and 150 mM NaCl. Peak fractions were pooled, spin concentrated to ~4 μM using the Amicon Ultra-4-10K column (Merck Millipore, Cat# UFC801024), and frozen in liquid nitrogen and stored at −80 °C. Approximately 50 μg total protein was obtained from 2 L of Sf9 cells. The Pol δ ^{Dead} mutant was purified as described for the wild-type protein.

Topo II α was purified as follows. A bacmid was generated by transforming DH10EMBacY cells with [pLDL189] pLib_TwinStrep-HRV3C-Topo II α, and the resulting bacmid was purified with the ZR BAC DNA Miniprep Kit (Zymo Research, Cat# D4049). Baculovirus was amplified in three 72-hour stages (P0, P1, P2) in Sf9 cells. TwinStrep-HRV3C-Topo II α was expressed in 1 L of Sf9 suspension culture by infection with 2 mL of P2 baculovirus for 65 hrs. Cells were harvested, pelleted by centrifugation, and flash frozen in liquid nitrogen. Cell pellets were thawed and resuspended in 100 mL of lysis buffer (25 mM HEPES-NaOH pH 7.5, 300 mM NaCl, 10% glycerol, 1 mM DTT) supplemented with 1x Pierce Protease Inhibitor EDTA-free (ThermoFisher Scientific, Cat# A32965) and lysed by Dounce homogenization. Lysate was cleared by ultracentrifugation at 35,000 rpm for 45 min at 4°C in a Beckman Type 70 Ti rotor (Beckman Coulter). Cleared lysate was incubated with 1 mL of Strep-Tactin®XT 4®Flow resin (IBA Lifesciences, Cat# 2-5010-010) for 1 hr at 4°C. The resin was washed with 3x10mL lysis buffer. The protein was eluted from the resin using 4 mL lysis buffer supplemented with 50 μg/mL HRV3C Protease for 2 hours at 4°C on a rotator, and flash frozen in liquid nitrogen. 2 mL of eluent was thawed and, diluted with 4 mL of no-salt buffer (25 mM HEPES-NaOH pH 7.5, 10% glycerol, 1 mM DTT) to reduce the NaCl concentration to 100 mM, and loaded on a Mono S 5/50 GL column (Cytiva, Cat# 17516801). The protein was eluted in 20 CVs off the column with a linear gradient of 100 mM – 1000 mM NaCl and eluted around ~300 mM NaCl. Peak fractions were pooled, spin concentrated to ~0.5 mL using the Amicon Ultra-4-10K column (Merck Millipore, Cat# UFC801024) applied to a Superdex 200 Increase 10/300 gel-filtration column (Cytiva, Cat# 28-9909-44) equilibrated in 25 mM HEPES-NaOH pH 7.5, 10% glycerol, 1 mM DTT and 150 mM NaCl. Peak fractions were pooled, spin concentrated to ~4 μM using the Amicon Ultra-4-10K column (Merck Millipore, Cat# UFC801024), and frozen in liquid nitrogen and stored at −80 °C. Approximately 300 μg total protein was obtained from 1 L of Sf9 cells.

GINS was purified as follows. A bacmid was generated by transforming DH10EMBacY cells with [pLDL113] pACEBac1_GINS-S6-6xHis, and the resulting bacmid was purified with the ZR BAC DNA Miniprep Kit (Zymo Research, Cat# D4049). Baculovirus was amplified in three 72-hour stages (P0, P1, P2) in Sf9 cells. GINS-S6-6xHis was expressed in 1/2 L of Tni suspension culture by infection with 2 mL of P2 baculovirus for 48 hrs. Cells were harvested, pelleted by centrifugation, and flash frozen in liquid nitrogen. Cell pellets were thawed and resuspended in 100 mL of lysis buffer (25 mM HEPES-NaOH pH 7.5, 500 mM NaCl, 10% glycerol, 1 mM DTT, 1 mM PMSF, 20 mM Imidazole) supplemented with 1x Pierce Protease Inhibitor EDTA-free (ThermoFisher Scientific, Cat# A32965) and lysed by Dounce homogenization. Lysate was cleared by ultracentrifugation at 35,000 rpm for 45 min at 4°C in a Beckman Type 70 Ti rotor (Beckman Coulter). Cleared lysate was incubated with 0.5 mL of Nickel-NTA resin (Qiagen 30230) for 1 hr at 4°C. The resin was washed with 3x10 mL lysis buffer. The protein was eluted from the resin using 5x0.5mL lysis buffer supplemented with 300 mM Imidazole, and flash frozen in liquid nitrogen. Eluent was thawed and, diluted with no-salt buffer (25 mM HEPES-NaOH pH 7.5, 10% glycerol, 1 mM DTT) to reduce the NaCl concentration to 150 mM, and loaded on a Mono Q 5/50 GL column (Cytiva, Cat# 17516601). The protein was eluted in 20 CVs off the column with a linear gradient of 150 mM – 800 mM NaCl and eluted around ~300 mM NaCl. Peak fractions were pooled, spin concentrated to ~0.5 mL using the Amicon Ultra-4-10K column (Merck Millipore, Cat# UFC801024) applied to a Superdex 200 Increase 10/300 gel-filtration column (Cytiva, Cat# 28-9909-44) equilibrated in 25 mM HEPES-NaOH pH 7.5, 10% glycerol, 1 mM DTT and 150 mM NaCl. Peak fractions were pooled, spin concentrated to ~3 μM using the Amicon Ultra-4-10K column (Merck Millipore, Cat# UFC801024), and frozen in liquid nitrogen and stored at −80 °C. Approximately 2 mg total protein was obtained from 1/2 L of Tni cells.

Fluorescent Labeling Using SFP Synthase

For AF647 labeling, 1 mg of Alexa Fluor 647 C2 maleimide (Thermo Fisher Scientific, cat # A20347) was reacted with 2 mg CoA-SH (Sigma-Aldrich, Cat # 234101-100MG) in 100 mM sodium phosphate pH 7.0 for 1 hour in the dark on a rotator at room temperature. The resulting product was separated from unreacted dye and unreacted CoA-SH by preparative HPLC using a reverse-phase Eclipse XDB-C18 column (PN 977250-102, 21.2 x 250 mm cartridge, 7 μm). The sample was run with a gradient of 0% (vol/vol)–50% (vol/vol) acetonitrile in 0.1% (vol/vol) TFA/water over 30 min at 10 mL/min. The AF647-CoA product eluted around ~36% acetonitrile. Peak fractions were pooled, lyophilized, and resuspended to a final concentration of 1 mM in DMSO. For LD555 and LD655 labeling, LD555-CoA and LD655-CoA was purchased from Lumidyne Technologies.

Site-specific fluorescent labeling of the S6 tag was performed in between the chromatography steps described above. Immediately following ion-exchange chromatography the molar concentration of the POI was estimated by the integrated intensity of the Abs280 reading on the FPLC chromatogram using a theoretical extinction coefficient. The POI was spin concentrated to ~0.5 mL and supplemented with 10 mM $MgCl_2$, a 2-fold molar excess of SFP synthase and a 10-fold molar excess of CoA conjugated dye. Reactions were incubated for 1 hour in the dark on a rotator at room temperature, then applied to a Superdex 200 Increase 10/300 gel-filtration column to separate unreacted fluorophore and SFP from the POI. The peak fractions were pooled and concentrated. Protein labeling efficiency was estimated based on absorbance measurements at 280 nm and the absorption peak for the respective dye. The biochemical activity of the labeled protein was tested following a published detailed protocol.[75]

Please cite this article in press as: Lynch et al., Metazoan lagging-strand DNA synthesis is distributive, Cell (2026), https://doi.org/10.1016/j.cell.2026.09.060

Ensemble Plasmid Replication Assay

All plasmid replication assays were conducted following a detailed protocol[75] using 4 ng/μL pBlueScript as the template DNA. Samples were taken at specified timepoints to monitor α^{32}P-dCTP incorporation or for western blotting.

Single Molecule Replication Assay

All single molecule experiments were conducted following a detailed protocol,[75] except for the following modifications. In the λ DNA tethering step, 20 pM of streptavidin^{AF647} (Thermo Fisher Scientific, Cat# S21374) was added to the streptavidin solution. Streptavidin^{AF647} spots were used as a fiducial marker for focusing immediately before starting imaging. After λ DNA tethering, DNA was licensed in HSS for 10 minutes. In this study, Replication Mix (10 μL of NPE, 10 μL of HSS, 3 - 6 μL of ELB-Sucrose, 1 μL of 600 ng/μL pBlueScript carrier plasmid DNA, 1 μL of ATP regeneration Mix, 1 μL of 70 μM FEN1^{mKikGR} or 1 μL of 11 μM RPA^{mKikGR}, and 1–3 μL of fluorescently labeled protein of interest = 30 μL total) was flowed into the microfluidic chamber at a rate of 10 μL/min. The reaction was then imaged continuously (10–30 sec/frame) without washing out the free fluorescently labeled protein. Thus, fluorescent protein (5–20 nM) was present in the replication reaction during the entire duration of the experiment unless indicated otherwise. Optimal replication efficiency was achieved when the single-molecule replication reaction contained equal volumes of NPE, HSS, and buffer. The concentrations of proteins examined in this study were estimated using quantitative western blots (see table below).

Protein of interest	Concentration in NPE (nM)	Concentration in replication reaction (nM)
Pol α	~2,100 nM	~700 nM
Pol δ	~3,000 nM	~1,000 nM

For single molecule "chase" experiments the same procedure described above was repeated through the licensing step. Following licensing Replication Mix was flowed into the microfluidic chamber to initiate the reaction. After the flow completed, the inlet tubing was changed to a Chase Mix without starting flow. The Streptavidin^{AF647} spots were used as a fiducial marker for focusing immediately before starting imaging. 15 minutes into the imaging acquisition the Chase Mix was flowed into the microfluidic chamber at 10 μL/min during continuous imaging.

When the replication reaction was chased with POI-depleted extract (Figure 3), samples from (1) the undepleted extract, (2) the depleted extract, and (3) the microfluidic flow-cell channel were taken for western blotting to validate the effectiveness of the chase in washing out the POI. To take the flow-cell sample, immediately after finishing the experiment, the inlet tubing was ripped out, and 1 μL was withdrawn from the flow-cell channel using a fine pipet tip. Initial attempts to chase with Pol α/δ-depleted extract resulted in substantial quantities of Pol α/δ from the initial Replication Mix persisting in the flow-cell (data not shown). Increasing the volume of the chase flow was necessary to wash out >99% of Pol α/δ. In Figure 3 the reactions were chased with 55 μL of Pol α/δ-depleted Chase Mix. We found that smaller 20 μL chase volumes were sufficient to block lagging strand synthesis when the Chase Mix was supplemented with catalytically dead polymerase as a competitor (Figures S3D–S3G). We note that it is critically important to measure the contents of the flow-cell in these types of experiments, as failure to effectively wash out a POI will lead to experimental artifacts.

Pol α/δ-depleted chase flow-cell samples from Figure 3 were monitored for CHK1 phosphorylation by Western blot (Figure S3C lanes 10 and 14). Flow cell samples were taken 30 minutes after the chase flow occurred. Using identical depletion conditions, we monitored CHK1 phosphorylation in ensemble plasmid replication assays in (1) mock-depleted, (2) mock-depleted supplemented with 5 μM aphidicolin, (3) Pol α-depleted, and (4) Pol δ-depleted extract (Figure S3C) and took samples for Western blotting at timepoints comparable to when the flow-cell sample was taken.

For chase experiments in Figure 4, replication was initiated in GINS-depleted extract supplemented with 20 nM GINS^{LD655} and ~367 nM RPA^{mKikGR}. The reactions were chased with GINS-depleted extract supplemented with ~367 nM RPA^{mKikGR} and DMSO, 50 μM aphidicolin, 100 μM CD437, or Pol α-depleted extract supplemented with 500 nM Pol α^{Dead}. GINS^{LD555} was used during the 500 nM Pol α^{Dead} chase to avoid spectral overlap (Pol α^{Dead} was labeled with Alexa Fluor 647). All reactions received a matched final concentration of 0.8% DMSO.

For chase experiments in Figures S4A–S4C GINS-depleted extract was supplemented with 20 nM GINS^{LD555} and ~367 nM RPA^{mKikGR}. Replication reactions were chased with GINS-depleted extract supplemented with DMSO or 100 μM CD437. 16.7 μM dUTP^{AZD647} was included in the chase flow. During this, GINS^{LD555} and RPA^{mKikGR} were imaged continuously. After 30 minutes the channels were washed with 50 μL DNA Buffer [10 mM Tris pH 8.0, 50 NaCl, 0.5 mM EDTA] flowed at 10 μL/min. The post-imaged dUTP^{AZD647} was aligned to the GINS^{LD555}/RPA^{mKikGR} movie using the Streptavidin^{AF647} fiducial spots.

The following settings were used for imaging FEN1^{mKikGR}: TIRF arm set to 9000 (~67°), 500 ms exposure, 10 s/frame, 8% 488 nm laser power (~60 μW power out of the objective, ~0.6 W/cm^2 power density), EM Gain Multiplier = 100, EM Conversion Gain = 1, 10 MHz at 16-bit read-out speed.

Please cite this article in press as: Lynch et al., Metazoan lagging-strand DNA synthesis is distributive, Cell (2026), https://doi.org/10.1016/j.cell.2026.09.060

The following settings were used for imaging both Pol α^{AF647} and Pol δ^{AF647}: TIRF arm set to 9000 (~67°), 500 ms exposure, 10 s/frame, 25% 640 nm laser power (~380 μW power out of the objective, ~3.8 W/cm^2 power density), EM Gain Multiplier = 100, EM Conversion Gain = 1, 10 MHz at 16-bit read-out speed.

The following settings were used for imaging RPA^{mKikGR}: TIRF arm set to 9000 (~67°), 500 ms exposure, 30 s/frame, 10% 488 nm laser power (~68 μW power out of the objective, ~0.68 W/cm^2 power density), EM Gain Multiplier = 100, EM Conversion Gain = 1, 10 MHz at 16-bit read-out speed.

The following settings were used for imaging GINS^{LD555}: TIRF arm set to 9000 (~67°), 500 ms exposure, 30 s/frame, 25% 561 nm laser power (~500 μW power out of the objective, ~5.0 W/cm^2 power density), EM Gain Multiplier = 100, EM Conversion Gain = 1, 10 MHz at 16-bit read-out speed.

The following settings were used for imaging GINS^{LD655}: TIRF arm set to 9000 (~67°), 500 ms exposure, 30 s/frame, 25% 640 nm laser power (~380 μW power out of the objective, ~3.8 W/cm^2 power density), EM Gain Multiplier = 100, EM Conversion Gain = 1, 10 MHz at 16-bit read-out speed.

The following settings were used for dUTP^{AZD647}: TIRF arm set to 9000 (~67°), 500 ms exposure, 10 s/frame, 25% 640 nm laser power (~380 μW power out of the objective, ~3.8 W/cm^2 power density), EM Gain Multiplier = 150, EM Conversion Gain = 3, 10 MHz at 16-bit read-out speed.

QUANTIFICATION AND STATISTICAL ANALYSIS

Single-Molecule Data Analysis

Each replication initiation experiment imaged 6–8 fields of view (FOVs) over the course of 45–60 minutes with a resolution of 10–30 seconds/frame. Each FOV typically contained 50–200 DNA molecules stretched to ~80% of their contour length. A suite of MATLAB scripts written in house were used to select and analyze data as described in our recent methods article.[75] Below we summarize the data analysis pipeline specific for the single molecule experiments analyzed in this study.

Selecting DNA Molecules for Analysis

Regions of interest (ROIs) corresponding to individual DNA molecules were selected manually based on the previews of DNA stained with SYTOX Orange (these were acquired before the start of the experiment). Only well-separated DNA molecules were used in the analysis.

Analyzing Polymerase Binding/Dissociation

To analyze the binding and dissociation of polymerases we employed an approach previously described in[81] for analyzing replication initiation factors. ROIs corresponding to polymerase binding events were selected from edges of FEN1 tracts, corresponding to the position of the replisome. For the analysis of fork-distal binding events (Figures S4H and S4I) ROIs corresponding to polymerase binding events were selected from FEN1 tracts behind the fork, corresponding to nascent DNA that the replisome had already moved past.

To analyze the binding and dissociation of polymerases on singly tethered molecules (Figures S1M–SIR), ROIs were also selected from the DNA Preview – singly tethered molecules appear as diffraction limited sources of SYTOX signal. Only singly-tethered molecules that replicated (displayed FEN1 signal) were analyzed. To minimize the number of ''non-productive'' binding events (Figures S1C and S1D) analyzed, we applied the following criteria: total FEN1 signal was integrated over time. This signal increases as the molecule replicates but eventually peaks and decreases presumably due to completion of DNA replication triggering FEN1 unloading. Polymerase binding events were therefore only selected from time points prior to the peak in FEN1 signal.

Changepoint Analysis

To identify the time when lagging strand synthesis ceased following chases in Figure 3, the edge of the FEN1 tract was fit with the following bilinear model in MATLAB:

$$b(x) = \begin{cases} a_1 x + b & x < x_0 \\ a_2 x + (a_1 - a_2) b x_0 & x \geq x_0 \end{cases}$$

where x_0 is the changepoint time, a_1 is the slope before the changepoint, a_2 is the slope after the changepoint, and b is the y-intercept. To confirm the robustness of the changepoint analysis we compared the goodness of fit to a linear model that lacks a changepoint term. The following monlinear model was fit to the same FEN1 tract:

$$m(x) = a_1 x + b$$

For each model we approximated the Bayesian Information Criterion (BIC) of the fit using:

$$BIC \approx n \log\left(\frac{sse}{n}\right) + K\, log(n)$$

where n is the sample size, sse is the sum of squared errors of the fit, and K is the number of parameters in the model.[82] We computed the difference of the BIC scores for each FEN1 tract:

$$\Delta BIC = BIC_{monolinear} - BIC_{bilinear}$$

where larger ΔBIC values indicate the FEN1 tract was better fit by the bilinear model. Comparing the ΔBIC values across the chases confirmed that the Pol α-depleted and Pol δ-depleted chases were better modeled by the bilinear fitting than the mock chase (data not shown).

CMG Velocity Analysis

To measure CMG velocity during/after the chase we fit the $GINS^{LD555}$ signal with a linear model in MATLAB and extracted the slope. Only timepoints that occurred after the chase were used for fitting.

Data Reporting

Details for statistical analysis are indicated in figure legends. Unless otherwise specified, error bars represent 95% confidence intervals (CI) for the median calculated using MATLAB's built in bootstrapping function. The exact meaning of the number 'N' reported in each figure is indicated in the figure legends (usually it refers to the number of replication forks or polymerase binding events). p-values were computed using the two-sample two-tailed Kolmogorov-Smirnov test function built into MATLAB. 'n.s.' denotes not significant, * = p value <0.05, ** = p value <0.01, *** = p value <0.001, **** = p value $\leq$0.0001.

Data Acquisition and Analysis Software

Nikon Elements AR (v5.20.02) was used to acquire the raw microscopy data. ImageJ Fiji (v2.1.0) was used to stabilize the raw microscopy movies. MATLAB (R2023a) was used to analyze the data using a suite of custom functions and scripts written in house.

ADDITIONAL RESOURCES

Raw data collected for this study is available here: https://doi.org/10.25740/sq803bx0564

Custom MATLAB scripts used to analyze the data are available here: https://doi.org/10.25740/sq803bx0564